3 Characterisation Techniques in Food Materials Science

Elliot Paul Gilbert[1], Amparo Lopez-Rubio[2] and Michael J. Gidley[3]

[1] *Bragg Institute, Australian Nuclear Science and Technology Organisation, Locked Bag 2001, Kirrawee DC, NSW 2232, Australia*
[2] *Novel Materials and Nanotechnology Laboratory, IATA-CSIC, Apdo. correos 73, 46100 Burjassot, Valencia, Spain*
[3] *Centre for Nutrition and Food Sciences, The University of Queensland, Brisbane QLD 4072, Australia*

3.1 INTRODUCTION

Food materials science seeks to investigate the relationship between the structure of food materials at the atomic or molecular scale to their macroscopic properties and behaviour. It includes elements of physics, chemistry, biology and mathematics; few would argue then that it naturally requires an interdisciplinary approach. The materials in question include proteins, carbohydrates and fats and the complexity of mixtures thereof. Challenges to the manufacturer may arise that result from consumer driven changes (e.g., lower fat foods) or inconsistency in supply due to environmental variations; the frequency with which the latter occurs is more likely to increase than decrease. To measure and control food structure, to make predictions of behaviour and to deliberately engineer consistent or new products, characterisation techniques are essential. The two books *Food Materials Science* by Aguilera and Lillford (Aguilera & Lillford, 2008) and *The Chemical Physics of Food* by Belton (Belton, 2007) along with the review *Understanding foods as soft materials* by Mezzenga et al. (Mezzenga et al., 2005) embody the richness of this area of science.

In this chapter, we describe no fewer than seven characterisation techniques that already find broad application in food materials science. The results from such techniques are discussed in conferences that are committed to enhancing our understanding of food materials science such as the biennial Food Colloids (Food Colloids, 2012) and triennial International Symposium on Food Rheology and Structure (ISFRS) meetings. However, not only are interdisciplinary approaches desirable to interrogate food materials but a broad arsenal of techniques is also essential, particularly if the material in question has some level of structural hierarchy.

As a rather simple example of this, and one that we will return to throughout this chapter, consider starch – a ubiquitous carbohydrate that provides up to 90% of the human nutritional energy in developing countries. A starch granule has a hierarchical structure; that is, it possesses characteristic structural features on a wide range of length scales. In vivo, starch granules are present within structural units with length scales of 10^{-4} m (cells) and $10^{-3} - 10^{-2}$ m

Food Materials Science and Engineering, First Edition. Edited by Bhesh Bhandari and Yrjö H. Roos.

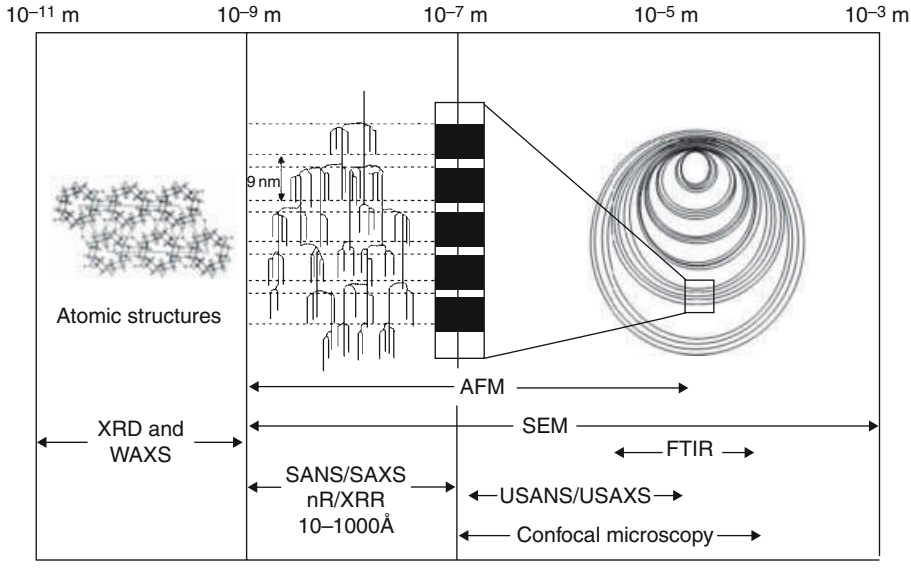

Figure 3.1 Experimental techniques described in this chapter and typical size range. The hierarchical structure of starch is shown spanning multiple techniques.
Source: adapted from Lopez-Rubio and Gilbert. Reprinted from *Trends in Food Science and Technology* 20, Neutron Scattering: A Natural Tool for Food Science and Technology Research, 576–586, Copyright (2009), with permission from Elsevier.

(tissues). Individual granules form on the 10^{-5} m scale but their size and shape varies depending on botanic origin. Growth rings occur on an order of magnitude below this. At 10^{-7} m are crystalline arrays, at 10^{-8} m are semi-crystalline lamellar repeats and interhelix separation occurs on the 10^{-9} m scale.

Figure 3.1 illustrates this range of starch structure and the corresponding experimental techniques described in this chapter. Thus, even for a 'simple' material such as starch, appropriate characterisation techniques should and must be employed to measure and understand structure from the atomic to the micron scale and beyond. It is certainly not the intent of this chapter to provide an exhaustive list of examples but to provide the reader with a basic understanding of the methods. These have, in turn, been illustrated with selected examples from food. In all cases, the reader is directed to texts or reviews that describe the methods in more detail. It is worthy to note, albeit beyond the scope of the current chapter, that one could develop a related figure encompassing the broad timescales necessary to describe food structure from milliseonds to hours (processing) and minutes to months (product stability). Such a figure would include, but not be limited to, techniques such as dielectric spectroscopy, quasielastic neutron scattering and differential scanning calorimetry.

3.2 NUCLEAR MAGNETIC RESONANCE (NMR)

3.2.1 General principles

Nuclear magnetic resonance phenomena have their origins within the nucleus of certain individual atom types, e.g. ^{1}H and ^{13}C, which possess a net 'nuclear' spin. The effects are only observed in a magnetic field ('magnetic') and involve the exchange of energy between

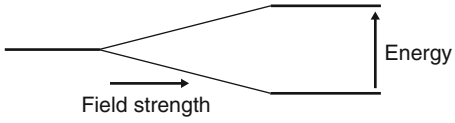

Figure 3.2 Schematic representation of nuclear magnetic resonance for a single nucleus.

at least two levels ('resonance'). The simplest form of NMR event involves two energy levels – this is the case for both ^{1}H and ^{13}C, the most commonly used NMR nuclei in food science, and is illustrated in Figure 3.2.

As for other forms of spectroscopy, the energy level gap determines both the frequency of observation and the sensitivity of the experiment. In the case of NMR, the energy level gap depends on the size of the magnetic field applied (Figure 3.2). To compare spectral positions (known as chemical shifts) for data collected on spectrometers of different magnetic field, chemical shifts are conventionally expressed in parts per million (ppm) of the applied field. One consequence of the dependence on magnetic field strength is that if the latter is varied then the NMR signal varies in frequency accordingly. This is the original basis for Magnetic Resonance Imaging (MRI), where a designed magnetic field gradient is applied across the sample to be imaged, leading to a unique magnetic field strength for each region within the sample. The location of ^{1}H nuclei within the sample can then be deduced from the measured spectral frequencies.

For the NMR property of nuclear spin, the energy level gap is very small. This means that the population of nuclear spins is only slightly less in the higher energy level than in the lower, resulting in facile exchange of nuclear spin between the energy levels ('resonance'). A consequence of this small difference in populations between energy levels is that NMR is markedly less sensitive than, e.g., ultra-violet or infra-red spectroscopy which have larger energy level gaps and hence a greater difference in population levels that are perturbed by the applied energy. For dilute nuclei such as ^{13}C, the low natural abundance (ca 1% compared to ^{12}C) reduces sensitivity even further. In order to achieve sufficient signal to noise ratios, a large number of energy inputs (known as pulses) and time domain signal acquisition steps are accumulated, prior to Fourier transformation, to reveal frequency domain spectral information. One reason for operating at high magnetic fields is therefore to maximise sensitivity, as typically fewer pulses and therefore shorter overall acquisition times are needed to generate adequate signal to noise ratios.

3.2.2 Chemical and physical information

There are two broad types of information that can be obtained from NMR spectroscopy. One is based on the effects of molecular structure and interactions (chemical effects) on the energy level gap, usually manifested by the chemical shift in high resolution spectroscopy. Although chemical shifts cover only a small fraction of the applied magnetic field (10 ppm for ^{1}H and 200 ppm for ^{13}C) effects are highly reproducible, being reliably measured to 0.001 ppm for ^{1}H and 0.01 ppm for ^{13}C by reference to chemical shift standards. Chemical shift values are primarily determined by the electronic environment of a nucleus with greater electro-negativity in the vicinity causing a downfield shift (higher ppm). For example, carbons and hydrogens in C–CH_2-C groups typically appear in the region of 1–2 ppm in ^{1}H spectra and 30–35 ppm in ^{13}C spectra; C-CH(OH)-C groups are in the region of 3–4 ppm and 60–80 ppm respectively; and C-CH(OH)-O groups are at 4–6 ppm and 90–110 ppm respectively. The high discriminating power of chemical shift effects and their reproducibility makes NMR a useful fingerprinting technique for the complex molecular compositions

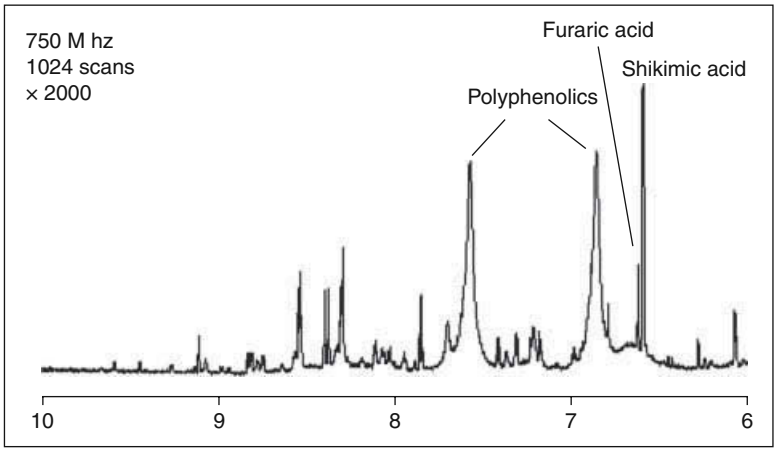

Figure 3.3 Partial ^{1}H NMR spectrum of mango juice showing many minor phenolic and related signals – total acquisition time 40mins (B.M. Flanagan and M.J. Gidley, unpublished).

present within many foods. Figure 3.3 shows an example of part of the ^{1}H spectrum of mango juice analysed directly without any pre-treatment. The ease of obtaining the spectrum and the ability to make some assignments based on chemical shift values is offset by the difficulty of assigning the many minor signals and the relative insensitivity of NMR compared with other methods such as mass spectrometry. Nevertheless, NMR assignment methods based on covalent connectivity (e.g., correlation spectroscopy – COSY) and through-space connectivity (e.g., nuclear Overhauser enhancement spectroscopy – NOESY) have been used to assign many signals in common complex food systems such as various juices, wines and oils, allowing subsequent non-invasive quantitative compositional analysis (Rossmann, 2001; Mannina et al., 2001; Anastasiadi et al., 2009).

The second general type of information available from NMR spectroscopy is based on relaxation properties and gives information on physical effects operating within the system. Following the application of energy to promote nuclear spins to the higher level (Figure 3.2), energy is lost as spins relax back to the lower energy level. There are two general types of relaxation. One is where energy is transferred to other nuclei within the system through dipolar interaction mechanisms; examples include T_2 and NOE effects that can operate either through bonds or through space (nm or less). This transfer of energy does not change the total magnetisation in the system, in contrast to T_1 mechanisms that involve loss of energy to the environment. Relaxation processes are modulated by both the electronic environment of nuclei and local molecular motions. Depending on the type of NMR experiment, the dominant mechanism of relaxation varies, as does the motional timescale that can be probed. An overview of relevant timescales is shown in Figure 3.4. For ^{1}H signals observed in solutions (e.g., Figure 3.3), observable relaxation effects are sensitive to very fast motions typical of small molecules tumbling in solution. More rigid molecules (e.g., gels or solids) relax so rapidly through ^{1}H – ^{1}H dipolar interactions, that conventional ^{1}H NMR spectra cannot be observed. Recent advances in magic angle spinning probes (see below) are now allowing high resolution ^{1}H spectra to be obtained (Diez-Pena et al., 2005; Brown, 2009), but information is still limited.

Molecular motions in the MHz and kHz frequency regions are more characteristic of (semi-)solid systems and can be probed via ^{1}H – ^{13}C dipolar interactions and ^{13}C $T_{1\rho}$ effects respectively using ^{13}C 'solid state' spectroscopy. For example, variable contact time

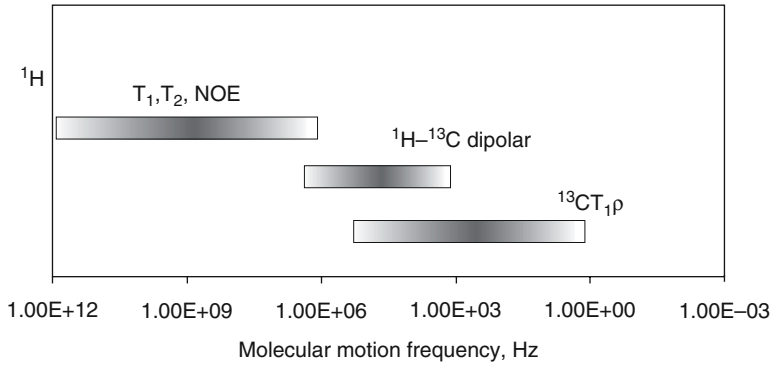

Figure 3.4 Schematic representation of the timescales of molecular motion that can be probed through different NMR relaxation mechanisms.
Source: BM Flanagan and MJ Gidley, unpublished, with permission from Elsevier.

experiments probe both the build-up of magnetisation by cross-polarisation from ^{1}H to ^{13}C via dipolar interactions and the subsequent decay of intensity via ^{13}C $T_{1\rho}$ effects, as will be discussed below.

3.2.3 High resolution NMR spectra from solids

The traditional application of NMR spectroscopy has been to molecules in solution where motion is fast enough to average any effects of orientation with respect to the magnetic field on observed chemical shifts, i.e., there is chemical shift isotropy. In addition, T_1 relaxation times are sufficiently short that the system returns to equilibrium rapidly and the next pulse of energy can be applied relatively quickly (typically of the order of one second) without saturating the system. In solids, T_1 values are longer, meaning that unreasonably long times are needed between pulses for full signal detection (typically of the order of minutes). In addition, dipolar interactions disperse energy across the system rapidly, leading to immeasurably broad signals. One advantage of the dilute nature of the ^{13}C nucleus (ca. 1% natural abundance) however is that ^{13}C – ^{13}C dipolar interactions are infrequent and hence weak. For ^{13}C NMR of solids, the strong ^{13}C – ^{1}H dipolar interaction can also be used to advantage as a route to selectively energising ^{13}C nuclei via adjacent protons, and allowing relaxation to occur through the ^{13}C $T_{1\rho}$ mechanism that typically occurs on millisecond timescales. Over the last thirty years, the application of NMR spectroscopy to solids and semi-solids such as found in most foodstuffs have become more frequent through the combined use of (a) cross polarisation (CP), (b) magic angle spinning (MAS), and (c) high power proton dipolar decoupling (DD).

Cross polarisation involves the energising of ^{13}C nuclei via ^{1}H nuclei and is most effective for carbons with directly attached hydrogens. The rate at which cross-polarisation occurs depends on the strength of the ^{13}C – ^{1}H dipolar interaction which, in turn, is dependent on molecular mobility. In practical terms, only relatively rigid (segments of) molecules undergo cross polarisation, effectively discriminating against mobile components within a sample. Magic angle spinning overcomes the effects of chemical shift anisotropy (i.e., the fact that each molecule has a different orientation with respect to the magnetic field resulting in different chemical shifts) inherent in solid samples because the magnitude of the anisotropy contains the term $3\cos^2\Theta - 1$. For the 'magic' angle of 57° 44', $3\cos^2\Theta = 1$

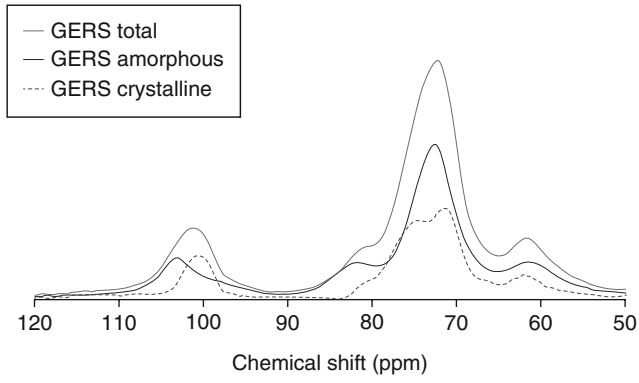

Figure 3.5 Typical CPMAS spectrum for a solid starch sample ('total') and computer-generated sub-spectra containing features of amorphous and crystalline material based on all intensity at 84 ppm being due to amorphous sites within the sample.
Source: Lopez-Rubio et al., 2008a, with permission from John Wiley & Sons.

so the anisotropy term becomes zero. Solid sample rotors in NMR machines are therefore inclined at the magic angle with respect to the magnetic field and are spun sufficiently fast that 'solution-like' averaging of molecular orientation is achieved. Finally, high power proton decoupling is used to repress dipolar spreading of energy, and to channel relaxation through the ^{13}C $T_{1\rho}$ pathway. The combined CP/MAS/DD approach (often abbreviated to CPMAS) has become the standard method for obtaining high resolution ^{13}C spectra from food materials with applications in, e.g., fat crystallisation (Bociek et al., 1985), polysaccharides such as starch (Figure 3.5, Gidley & Bociek, 1985; Tan et al., 2007) and gelling agents, protein-based food ingredients (Kealley et al., 2008) as well as complex whole foods.

One particularly powerful application of solid state NMR spectroscopy is to quantify sub-crystalline order in solid samples. The characteristic length scale for NMR is very short (nm or less), whereas the benchmark method for determining solid state structure (X-ray diffraction) requires structural register on at least a 10 nm length scale. Many natural and fabricated structures found in foods have limited, if any, crystallinity but are thought to contain molecular order. Examples in foods include protein and polysaccharide gels / fibres, starches and plant cell walls. Figure 3.5 illustrates the analysis of starch-based samples. The observed spectrum is split into sub-spectra representing 'crystalline' and 'amorphous' components based on the finding that model crystalline materials have no detectable intensity at 84 ppm (Tan et al., 2007). The spectral features of a model amorphous material (e.g., after thorough cooking and drying) are subtracted from the observed spectrum until intensity at 84 ppm is zero. The spectral intensity required for subtraction quantifies the 'amorphous'-to-'crystalline' ratio which has been shown to equate to X-ray quantification for most uncooked starch granules provided an imperfect crystallite model is used (Lopez-Rubio et al., 2008a). Following subtraction of amorphous features from starch spectra, a 'crystalline' sub-spectrum is generated. The chemical shifts for this spectrum – particularly for the signal at ca 100 ppm – are characteristic of the crystal polymorph; the relatively broad signals (e.g., Figure 3.5) are consistent with a low level of crystalline register as also observed by X-ray diffraction. Similar polymorph identification and quantification has been achieved for cellulose in isolated form (Atalla & VanderHart, 1984), in composites with

other polysaccharides (Whitney et al., 1995), and as found in, for example, fruit or vegetable cell walls (Foster et al., 1996).

3.2.4 Mobility-resolved NMR spectroscopy

A major advantage of NMR spectroscopy is that the operator has control over how and when energy is transferred to the sample, which mechanisms are available for energy evolution, and how energy is lost to the environment. This is possible through a wide range of sophisticated 'pulse sequences' that control the timing, power, and selectivity of energy inputs into the system. A practical consequence is that a single sample can be analysed by a number of complementary techniques to build a more complete picture of the molecular basis for the material's observed macroscopic behaviour. One example of particular value to the semi-solid systems frequently encountered in food is that of mobility-resolved spectroscopy (Gidley, 1992) in which a series of spectra – typically ^{13}C – are acquired under conditions that detect signals with characteristic molecular mobility properties. This allows the association of specific molecules or parts of molecules with defined molecular mobility regimes within intact samples. Examples of applications include a number of food gels (Gidley, 1989; 1992), plant cell walls (Foster et al., 1996), and proteins in limited water (Kealley et al., 2008). For plant cell walls, rigid cellulose fibres are only observed in CPMAS spectra whereas the more flexible pectin network has a sufficiently short T_1 value to also be detected by conventional direct polarisation (DP), provided that high power proton decoupling is also applied to prevent energy spreading via T_2 mechanisms. A further distinction can be made (Foster et al., 1996) for the pectin network between backbones, that are restricted in their ability to re-orient and hence require magic angle spinning to simulate motional averaging (DPMAS experiment), and side chains that re-orient sufficiently rapidly themselves that motional averaging occurs (DP or conventional high resolution experiment).

3.2.5 Probing water 'pool' sizes using ^1H T_2 properties

Water is often the major component in foods – even in solids. Techniques for characterising the state of water within intact food materials are important in understanding microenvironments that contribute to bulk materials' properties. The fact that water, as a very small molecule, has different relaxation properties to other food components has been exploited to develop methods for characterising the pool size of water within complex materials. The principle involved is that liquid water has a comparatively long $^1HT_2$ (several seconds), whereas materials such as emulsifiers/oils found at the droplet surface of water-in-oil emulsions or biopolymers that structure aqueous-based (semi-)solids have much shorter values (milliseconds or microseconds). Water protons are mobile and in most cases will be present at the interface/surface for a fraction of time that is dependent on the water pool size and potentially the local viscosity. When water protons visit a surface, they can exchange energy with the much faster-relaxing molecules present there. Thus measurement of water $^1HT_2$ values in the presence of a surface in comparison with the absence of the surface gives a measure of the proportion of time that a water proton spends adjacent to the surface and hence the size of the pool in which it is contained (Figure 3.6).

This method has been found to be so useful for characterising water-in-oil emulsion droplet sizes (Johns & Hollingsworth, 2007) that it has become the industry standard method for defining droplet size distributions of critical importance to materials, and is one of the few examples where NMR equipment is used routinely within food processing

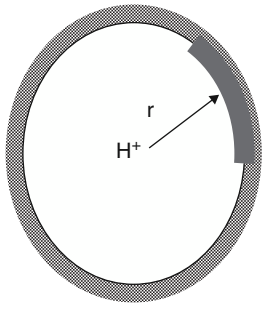

Figure 3.6 Schematic illustration of the mechanism that determines water $^1HT_2$ values. The distance 'r' that a ^1H nucleus is from a protein surface defines the fractional time spent within the sphere of influence of fast-relaxing protein compared with slow-relaxing bulk water.

operations. Other applications of NMR are typically restricted to the laboratory as equipment is expensive and dedicated trained operators are required.

3.2.6 Integration of techniques to study protein denaturation and glassing

For materials science and engineering in particular, there is an opportunity to link macroscopic materials behaviour to underlying molecular mechanisms. Kealley et al., and Huson et al., used a suite of NMR techniques on soy glycinin (Kealley et al., 2008; Huson et al., 2011) to investigate the influence of moisture and thermal denaturation on molecular mobility above and below the calorimetric glass transition. Variable contact time experiments suggest major effects on the molecular motion for all backbone and side-chain sites on passing through the calorimetric glass to rubber transition, particularly for native glycinin. In addition, the relaxation in denatured glycinin is faster than native glycinin. The nature of mobile segments, probed through DPMAS experiments, show that with increasing moisture, signals become both more intense (showing that the relative amount of the mobile fraction increases) and sharper (showing that motional averaging on the MHz timescale is occurring). For both samples, mobilisation of the backbone is assessed as being the major effect of passing through the calorimetric glass to rubber transition. The greater intensity at lower water contents for native versus denatured glycinin suggests that there are more relatively mobile molecular segments in the native protein than after denaturation. Comparison of the $^1HT_2$ distribution shows longer T_2 values for the native protein; this is interpreted as being due to a greater available surface for water exchange (Figure 3.5) to occur after denaturation, thereby reducing average water pool sizes at the same content compared with native glycinin.

3.3 FOURIER TRANSFORM INFRA-RED (FT-IR)

In the food science area, Fourier-transform infrared (FT-IR) spectroscopy has been mostly employed for rapid routine analyses of various food samples such as milk, meat or juices to enable testing for adulteration, to prove that products comply with regulation or to fix the price of the product according to established compositional standards (Cordella et al., 2002). Van der Woort (van de Voort, 1992) provides an excellent review of the technique

illustrating the potential to understand structural changes and perform time-resolved experiments in food-related systems.

Infrared spectroscopy explores the interactions between the atoms and their vibrations and, thus, it is a valuable technique for the study of molecular structure. An infrared spectrum is commonly obtained by passing infrared radiation through a sample and determining the fraction of incident radiation that is absorbed at a particular energy. The vibrational frequencies are determined by the chemical conformation, the mass of the atoms, and eventually by the associated vibronic coupling. The spectrum identifies at which wavelengths the sample absorbs in the infrared region, and allows an interpretation of which bonds are present (Hambleton et al., 2008). The width and intensity of the spectral bands, as well as the position of the peaks, are all sensitive to environmental changes and to molecular conformation. From a general point of view, spectroscopic techniques yield structural information that constitutes a molecular fingerprint of the sample.

An understanding of molecular symmetry and group theory is important when initially assigning infrared bands. A detailed description of such theory is beyond the scope of this chapter, but symmetry and group theory are discussed in detail in Vincent (2001) and Atkins & de Paula (2002). Fortunately, it is not necessary to work from first principles each time a new infrared spectrum is obtained, as the frequencies of infrared absorption for most common types of atomic bonds and functional groups are well-known and described in the literature (Stuart, 2005).

Some of the advantages of the technique are that it is a non-destructive technique and that virtually any sample in any state can be studied. Moreover, no special sample preparation is required thus constituting a simple, non-invasive and reliable method necessitating minimum labour and chemicals for the measurement of food properties (Isiguro et al., 2005; Khurana et al., 2007; Monaci et al., 2007).

The samples can be measured either in transmission or in reflectance mode. Transmission spectroscopy is the oldest and most straightforward infrared method. This technique is based upon the absorption of infrared radiation at specific wavelengths as it passes through a sample. It is possible to analyse samples in the liquid or solid forms when using this approach. When using transmission cells it can be useful to know precisely the path-length of the cell, particularly for quantitative measurements.

Reflectance techniques may be used for samples that are difficult to analyse by the conventional transmittance methods. Reflectance methods can be divided into two categories. Internal reflectance measurements can be made by using an attenuated total reflectance (ATR) cell in contact with the sample (e.g., Kealley et al., Biomacromolecules 2008). There is also a variety of external reflectance measurements which involve an infrared beam reflected directly from the sample surface. In external reflectance, the energy that penetrates one or more particles is reflected in all directions and this component is called diffuse reflectance. In the diffuse reflectance (infrared) technique, commonly called DRIFT, a powdered sample is mixed with KBr powder (Stuart, 2005). This technique has proved useful as an alternative, rapid method to facilitate the calculation of the degree of esterification of commercial pectin samples (Gnanasambandam & Proctor, 2000).

As mentioned previously, infrared spectroscopy has been a common qualitative technique for the identification and verification of chemical compounds in foods and also for quantitative analysis, as the intensities of the bands in the IR spectrum are proportional to concentration, according to the Beer–Lambert law. When quantification of substances in food products is required, chemometric techniques are usually applied using one or a combination of statistical approaches like principal component analysis (PCA) or partial least-squares (PLS)

(Shim et al., 2008). These techniques are based on taking the infrared spectra from samples of known composition to predict the concentration in spectra of unknown composition.

Protein structures and their conformational changes with temperature or the addition of different salts can also be studied using FT-IR. This can be achieved through the analysis of the second derivative of the spectra followed by curve fitting using a Gaussian profile (Curley et al., 1998). Changes in components of the amide I and II regions are analysed by these means and can be correlated with changes in the component proteins' secondary structure.

Whey proteins and their properties have been extensively studied because of their importance as food ingredients. The most studied whey protein has been ß-lactoglobulin. The structural properties of this protein, as well as the conformational changes as a function of time, temperature and pH have been studied using FT-IR and the results were found to be in reasonable agreement with other techniques such as X-ray crystallography (Fang & Dalgleish, 1997). Similarly, the structural changes of the other major whey protein, i.e., α-lactalbumin, as a function of pH and temperature were also analysed with this spectroscopic technique. Both proteins play an important role in the stabilisation of oil-in-water emulsions and food gels and their structure-related properties can be used to optimise industrial processes (Fang & Dalgleish, 1998).

A further interesting study dealing with proteins and FT-IR was carried out by Saguer and co-workers (2008). The technique was used to elucidate the molecular basis of structure–functionality relationships of porcine plasma proteins in the solution and gel states at varying pH. At room temperature, porcine plasma proteins aggregate as a function of decreasing pH; this is accompanied by a decrease in the intensity of amide I bands at 1652 cm^{-1} in the infrared spectra of the protein solution (assigned to α-helix) and at 1688/1638 cm^{-1} (assigned to intramolecular antiparallel ß-sheet) along with an increase in the band at 1644 cm^{-1} (assigned to an unordered or random structure). Texture and water-holding capacity are also very sensitive to pH. The results indicate that the lower the remaining native secondary structure and the faster the heat-induced aggregation (observed by FT-IR spectroscopy) with decreasing pH, the weaker are the gels and the greater is their exudation behaviour (Saguer et al., 2008).

Changes in the short range order of starches as a consequence of processing or simulated digestion can also be followed using FT-IR spectroscopy. Using a combination of techniques it was found that, during in vitro digestion of processed high amylose starch, an increase in crystallinity and molecular order takes place (Lopez-Rubio et al., 2008). The ratio between the bands at 995/1022 cm^{-1} have been used to quantify the degree of order in starches (Sevenou et al., 2002). Figure 3.7 shows the FT-IR spectra in the region 800–1200 cm^{-1} for processed high amylose starch at various times of digestion. In this figure an increase in the absorbance of the band at 995 cm^{-1} and a decrease in the band at 1022 cm^{-1} with digestion time are observed (see arrows). The two bottom spectra of Figure 3.7 with very similar spectral profiles correspond to the control samples at 0 min and after 18 h in the digestion medium without enzyme, confirming that, in the absence of α–amylase, the molecular order of starch is largely unaffected (Lopez-Rubio et al., 2008a).

The FT-IR technique also has great potential to study the structure of food packaging and to characterise mass transport properties. Polymeric food packages are designed to preserve foods and minimise interactions with the surrounding environment. The structure of the package determines to a large extent the kinetics of mass transport as the crystalline parts are considered to be largely impermeable. Therefore, changes in the crystalline structure as a consequence of, for instance, food preservation processes, can affect the gas permeability of the materials compromising the shelf-life of the packaged product. Ethylene-vinyl

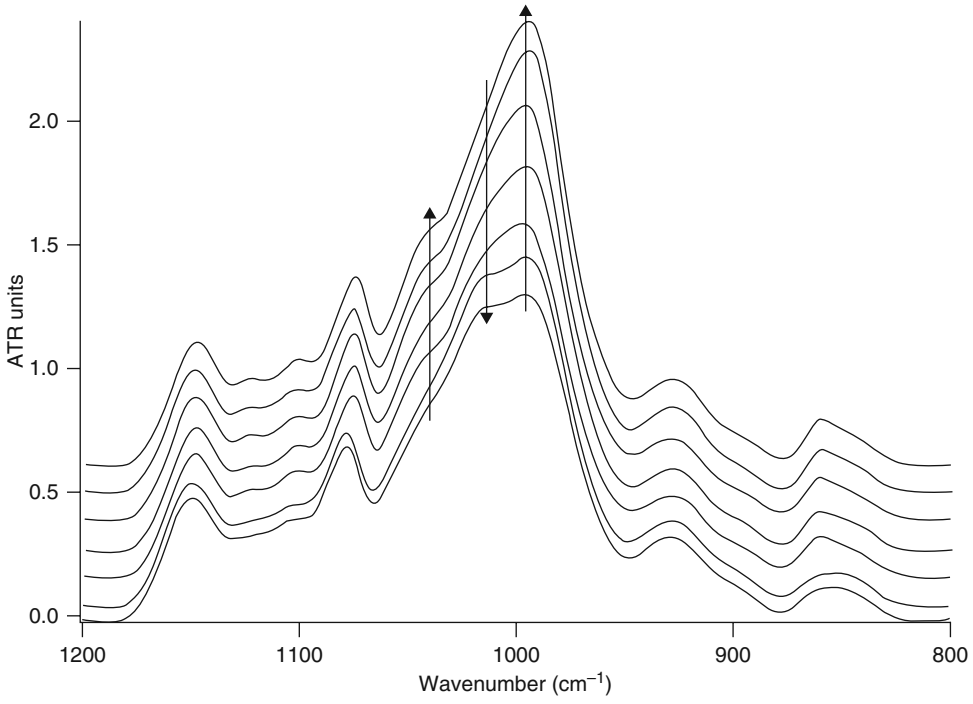

Figure 3.7 FT-IR spectra of processed high amylose starch as a function of digestion. From bottom to top: 0 min (control), 18 h (control), 5 min, 30 min, 4 h, 8 h, 18 h. Arrows indicate the evolution of intensity of the considered IR bands.
Source: reprinted with permission from López-Rubio, A., Flanagan, B.M., Shrestha, A.K., Gidley, M.J. and Gilbert, E.P. (2008b). Molecular rearrangement of starch during in vitro digestion: toward a better understanding of enzyme resistant starch formation in processed starches. *Biomacromolecules* 9, 1951–1958. Copyright 2008, the American Chemical Society.

alcohol (EVOH) copolymers are a family of semi-crystalline materials with excellent barrier properties to gases; they are consequently widely used as barrier layers in multilayer structures in various packaging designs for foodstuffs. The presence of EVOH in the packaging structure is significant to food quality and safety because it reduces the ingress of oxygen and the loss of aroma components during extended package shelf-life. However, humid sterilisation processes used for the preservation of foods cause a reduction in EVOH barrier properties, which has been ascribed to a significant decrease in their crystallinity (López-Rubio et al., 2003). In previous work, FT-IR was found to be exceptionally valuable as a characterisation tool for these materials due to the high sensitivity of the technique to simultaneously detect changes in crystallinity and water sorption levels.

Although flavour compounds are minority constituents of foodstuffs, small alterations in the quantity or relative presence (aroma imbalance) of them can produce organoleptically detectable changes resulting in consumer rejection. The permeation of low-molecular weight chemical species is generally envisaged as a combination of two processes, i.e., sorption and diffusion. A permeate gas is first dissolved into the upstream face of the polymer film, and then, undergoes a molecular diffusion to the downstream face of the film where it is desorbed into the external phase again. A sorption-diffusion mechanism is thus applied, which can be formally expressed in terms of permeability (P), being the product of

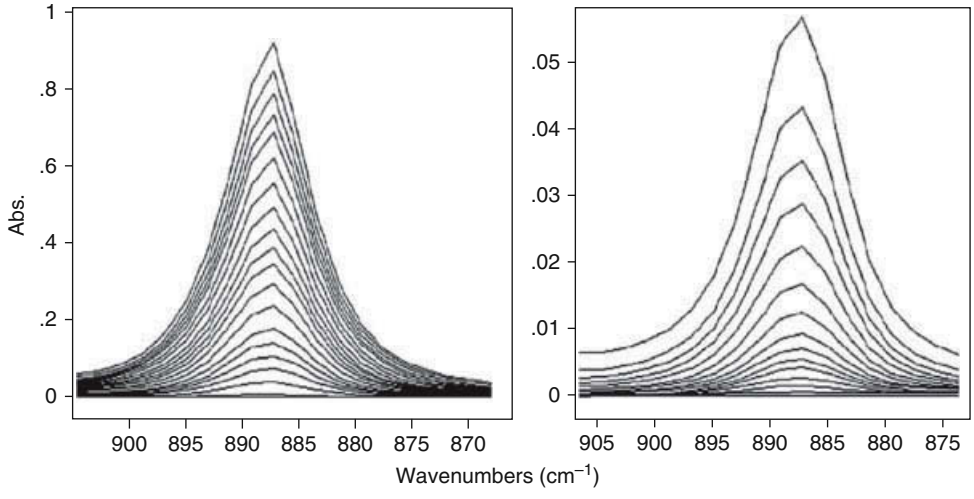

Figure 3.8 Subtracted FT-IR spectra in the range of the limonene C–H deformation mode recorded during desorption from 80 (left) and 10 (right) micron LDPE films.
Source: Reprinted from Cava et al., 2005 with permission from Elsevier.

the solubility (S) and diffusion (D) coefficients, as defined by Henry's and Fick's laws, respectively (Crank, 1975).

Fruit juices are foodstuffs where flavour is one of the most appreciated features, and consequently, the loss of volatile compounds is a major concern to manufacturers. The application of simple transmission FT-IR methodologies to determine transport properties have significant potential and, as an example, the technique has been used for the determination of the diffusion coefficient (D) of citric juice aroma components in polyethylene (Cava et al., 2004). This was done by fitting the desorption data as a function of time to the corresponding solution of Fick's second law after making several basic assumptions.

Generally, the FT-IR technique offers the advantages, when measuring transport properties, of being capable of assessing the different kinds of interactions that can be established between the polymer and the penetrant at different stages of sorption, by way of analysing band shifts and band shape changes. Furthermore, FT-IR is also advantageous compared to, for example, conventional gravimetry or gas chromatography, because it is a time-resolved technique and very thin films can be easily and precisely evaluated.

A significant advantage of the FT-IR technique is presented in Cava et al. (Cava et al., 2004), illustrating the possibility of studying mixtures of aroma compounds and their-interactions compared to gravimetric measurements. To illustrate this phenomenon, the diffusion of components in binary and ternary mixtures with equal volumes of the various components was studied. The different types of interactions between the mixture constituents and the polymer can induce changes in their diffusion coefficients and, therefore, the values calculated for the pure components do not necessarily apply. Another work from Cava et al. (2005) studied the effect of a number of relevant factors that are not usually considered in the analysis of the transport properties of aroma components, in this case limonene, through food packaging LDPE films. These factors were sample thickness, permeant concentration and the outer medium. From the results, a surprising reduction in diffusion (D) and permeability (P) coefficients with reducing film thickness were found, which are most likely attributed to morphological differences arising during cast film extrusion. Figure 3.8 shows FT-IR spectra

in the range of the limonene C–H deformation mode recorded during desorption from the films with different thickness. Finally, the sorption kinetics of limonene in LDPE were found to be much slower, when the polymer was put in contact with a pressed orange juice (similar to a real juice packaging case), than when it was put in contact with the pure volatile. A remarkable observation arising from this work is that the diffusion coefficient of limonene in LDPE can be found to vary for up to two others of magnitude depending on the testing conditions, primarily as a function of limonene concentration but also polymer morphology; consequently, these observations may account for some of the extensive variability reported for this permeant in the literature.

3.4 X-RAY POWDER DIFFRACTION

In a gas or liquid, the atoms move around in an available volume and the positions of the atoms lack long-range order. In a solid, however, while the atoms move, they do so about their equilibrium positions. In so-called crystalline solids, the mean positions of the atoms have a regularity (unit cell) that persists over large distances along three or more principal directions known as the basis (or lattice) vectors. Since this book specifically addresses food materials science, the reader is most likely to come into contact with powder (as opposed to single crystal) samples. These are polycrystalline materials composed of crystallites with either a uniform distribution of orientations or perhaps a sample with some degree of preferred orientation. Such samples may be investigated with X-ray powder diffraction (XRD).

When a beam of X-rays is directed to a material, some of the radiation will be absorbed, some will emerge in a new direction with or without a change in energy and the remainder will pass through the material unaffected. X-rays that emerge in a new direction are said to be scattered. The scattering of X-rays from atoms arises through interaction with the atoms' electrons and generates secondary spherical waves that emanate from the electron. Since crystals possess regularity in atomic positions, a regular array of waves is generated throughout the material which may constructively or destructively interfere.

The constructive interference results in 'reflections' or diffraction peaks. Bragg's Law – $2d\sin\theta = n\lambda$ – rather intuitively relates the scattering angles at which these reflections occur to the separation between the associated planes of atoms that gives rise to them as if the waves have been reflected from them (Figure 3.9). Here d is the spacing between the diffracting planes of atoms, θ is the angle of incidence on the sample (thus 2θ is the scattering angle through which the beam has changed direction), n is an integer and λ is the wavelength of the beam. Typical X-ray wavelengths used for crystallography are of the order of 1 Å – the 'standard' being 1.5418 Å corresponding to the average Kα line for copper – which is of the same order of magnitude as the spacing, d, between planes in the crystal.

The orientation of the diffraction planes is identified by its three Miller indices (h, k, l); a reflection is said to be *indexed* when its Miller indices (or, more correctly, its reciprocal lattice vector components) have been identified from the known wavelength and the scattering angle 2θ. Such indexing gives the unit-cell parameters, the lengths and angles of the unit-cell, as well as its space group. Since Bragg's law does not interpret the relative intensities of the reflections, however, it is generally inadequate to solve for the arrangement of atoms within the unit-cell; for that, a Fourier transform method must be carried out. XRD can be considered for any one of the following cases: (a) to 'fingerprint' the sample by comparing it with previously recorded diffraction patterns (ie is phase 'X' present or not?); (b) to calculate basic structural parameters such as unit cell by direct fitting of peaks using

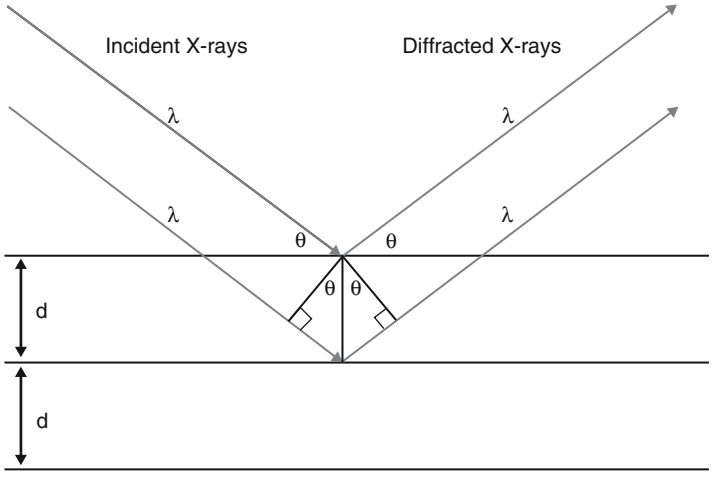

Figure 3.9 Bragg peaks are observed in XRD as a result of constructive interference between the scattered radiation from crystal lattice planes separated by a characteristic distance, d.

Bragg's Law or c) to refine fully the structure. For an excellent primer on XRD, the reader is directed to Cullity (Cullity, 1978).

Wide-Angle X-ray Scattering (or WAXS) is related to XRD. In practice, WAXS tends to be performed in transmission geometry, i.e., measuring the beam after being transmitted through the sample, whereas XRD may be performed in transmission or reflection geometry. In practice, for polycrystalline samples, differences in the XRD measured in transmission and reflection geometry are evident only for samples with some preferential orientation. As the degree of long-range order decreases in a crystalline material, the diffuse scattering increases and Bragg peaks increasingly widen leading to the generation of broad undulating features characteristic of amorphous materials. Usually, the term WAXS is used in connection with diffuse scatterers (i.e., less than perfect crystalline materials), while the term XRD is used for polycrystalline samples.

It is worthwhile noting that the terms scattering and diffraction are sometimes used rather loosely and interchangeably. Scattering may be thought to arise as a result of the interaction of radiation with an individual atom (via the electron for X-rays or nucleus for neutrons); diffraction then arises as a result of interference of these primary waves. However, in common parlance, diffraction more generally describes the scattering from crystalline materials and 'scattering' defines all other cases. The determination of the arrangement of atoms within a crystal resulting from the scattering from X-rays of the electrons within the crystal is referred to as X-ray crystallography.

The application of X-ray diffraction to food-based systems extends to any material in which crystallinity or some degree of long-range order exists. A classic example is that of starch. Starch granules, depending on their botanical origin and composition (amylose/amylopectin ratio, amylopectin branch length), exhibit two types of X-ray diffraction patterns, which are associated with two crystalline polymorphic forms. The A-type is mainly found in cereal starches and the B-type observed in tubers and high amylose starches (Zobel, 1988; Buléon, 1998a) (Figure 3.10). These consist of left-handed parallel stranded double helices packed in monoclinic and hexagonal unit cells for the A and B-type crystallites, respectively. Figure 3.10 shows powder patterns for two such starches along with vertical

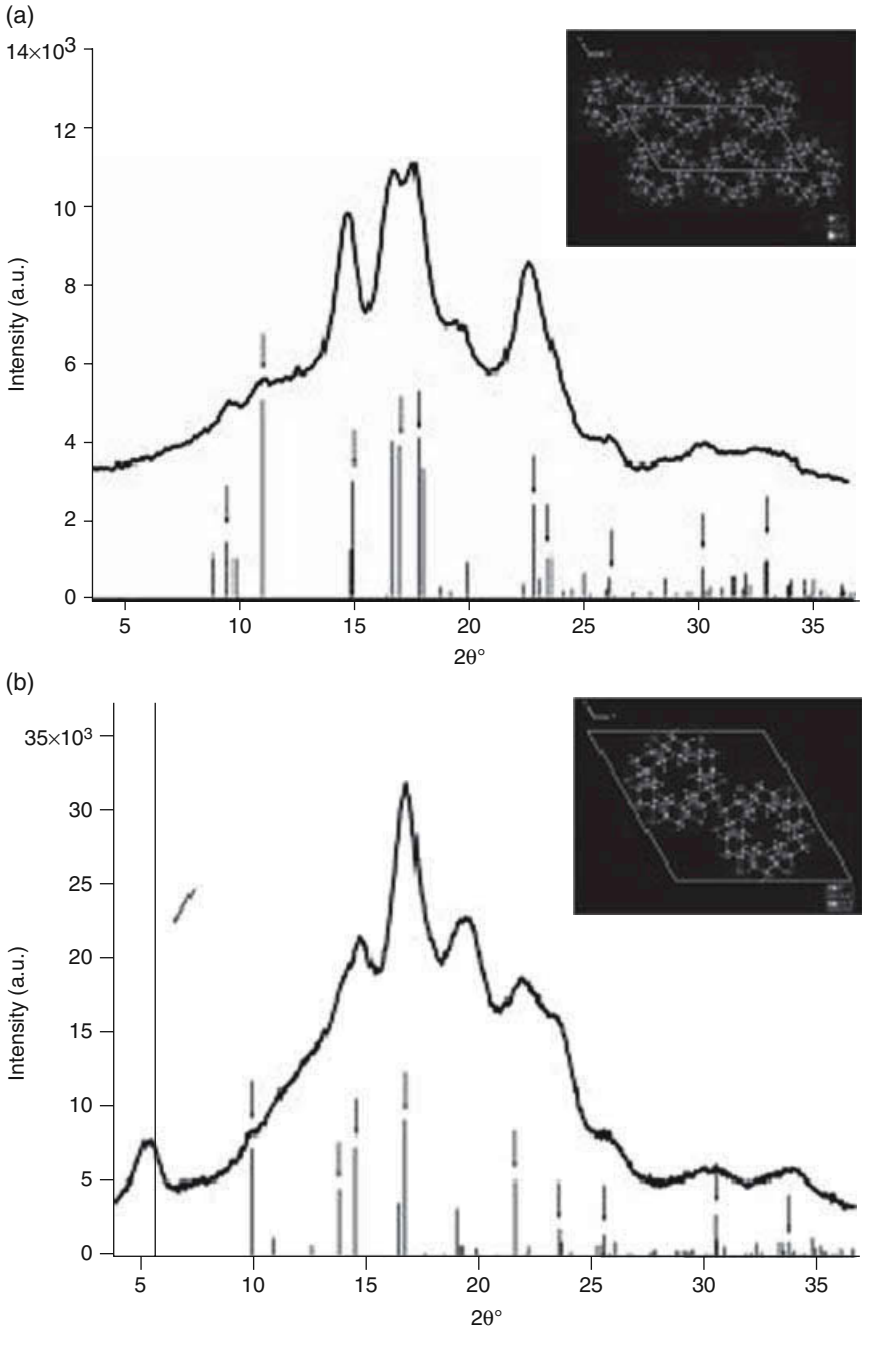

Figure 3.10 (a) XRD patterns of Nippon Bare with the associated A-type crystal powder pattern and unit cell. (b) XRD patterns of Gelose 80 with the associated B-type powder pattern and unit cell. Arrows indicate the reflections selected for fitting to enable the determination of crystallinity.
Source: from Lopez-Rubio et al., 2008a, with permission from John Wiley & Sons.

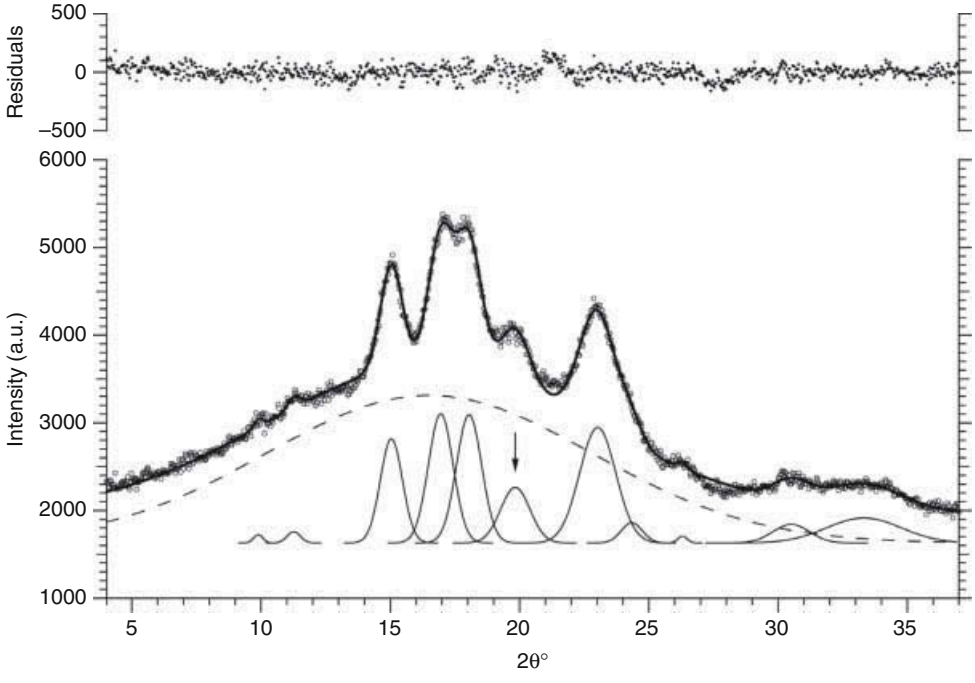

Figure 3.11 XRD from Penford wheat starch. The area under the dashed curve represents the amorphous content of the starch and the sum of the areas under the peaks, fitted with a Gaussian function, corresponds to the crystalline content. Arrows indicate the contribution from V-type crystallinity.
Source: from Lopez-Rubio et al., 2008a, with permission from John Wiley & Sons.

bars representing the position and relative intensity of the unit cell reflections for perfect A and B-type crystal polymorphs. The so-called C-type has been demonstrated to arise from coexisting A and B crystals in the granule (Buléon, 1998b). Another crystal polymorph is often observed in granular starches, the so-called V-type, which, in contrast with the double helical nature of the A and B crystal structures, has been demonstrated to arise from single amylose helices some of which are complexed with endogenous granular lipids (Morrison et al., 1993). Similar structures arise from the complexation of starch with alcohols and flavour compounds (Nuessli et al., 2003; Le Bail et al., 2005).

The degree of crystallinity, which can be defined as the percentage of the crystalline regions with respect to the total material, has been traditionally based on the two phase concept, which assumes that relatively perfect crystalline domains (crystallites) are interspersed with amorphous regions. However, it is well known that polymeric structures encompass intermediate crystalline objects, chain folding, lamellar crystalline growths, lattice dislocations, and other phenomena. According to the crystal defect concept of polymer structure, a portion of the X-ray scattering from the crystalline domains is diffuse and contributes to the so-called amorphous background; this brings into question the simple method of estimating the degree of crystallinity by separating the diffraction pattern into sharp (crystalline) and diffuse (amorphous) components (Morrison et al., 1993). Lopez-Rubio et al. recently reported on an improved method for the determination of crystallinity in starches using a crystal defect model and correlated this with high resolution ^{13}C nmr (Lopez-Rubio et al., 2008a) (Figure 3.11). Johnson et al. (Johnson et al., 1980) have applied XRD to determine crystallinity in gels.

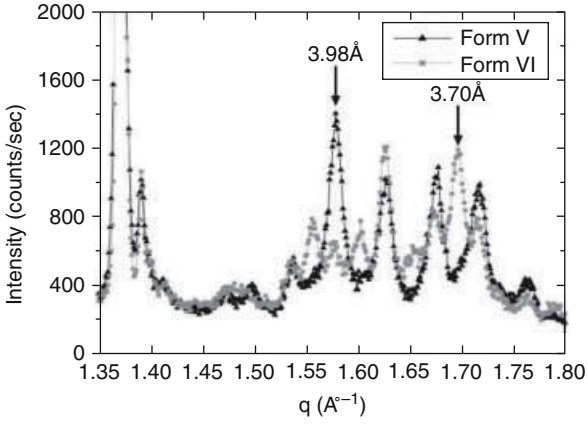

Figure 3.12 Cocoa butter form V and form VI polymorphs.
Source: Sarah E. Guthrie, Gianfranco Mazzanti, Stefan H. J. Idziak, X-ray phase identification of chocolate is possible without the removal of sugar, *Eur. J. Lipid Sci. Technol.*, 2005, 107, 656–659. Copyright Wiley-VCH Verlag GmbH & Co. KGaA. Reproduced with permission.

XRD has been applied to study a wide range of food-based materials (Michel & Sagalowicz, 2008). The polymorphs of cocoa butter crystals have been identified and optimised and the impact of bloom elucidated in chocolate (Figure 3.12) (e.g., Guthrie et al., 2005; Kinta et al., 2005; Le Reverend et al., 2008; Rogers et al., 2008). Soy protein isolate-clay nanocomposites have been investigated for their application for novel food packaging materials (Chen & Zhang, 2006). Manno et al. and Aravind et al. have used the technique as a fingerprinting method to identify the presence of inulin added to durum wheat pasta (Manno et al., 2009; Aravind et al., 2012). Haque and Roos have applied XRD to investigate the influence on crystal structure in lactose-protein mixtures as a result of differences in drying protocol (Haque & Roos, 2005).

3.5 SMALL ANGLE NEUTRON & X-RAY SCATTERING (SANS AND SAXS)

To investigate the properties and their effects on the final characteristics of a food product, it is valuable to maintain the surrounding environment as close as possible to the original conditions. In this sense, small-angle scattering possesses particularly attractive attributes. Except in some cases where synchrotron X-radiation is used, small-angle scattering constitutes a non-invasive technique that enables the study of materials under realistic conditions including partial hydration, gels and solutions.

Due to their inverse relationship, the scattering at small angles gives rise to structural details over larger length scales than may be obtained from conventional powder diffraction instruments and on a scale from approximately one to several hundred nanometres. This ‘nano’-size range transcends disciplines and extends across proteins (biology and medical sciences), emulsions, microemulsions (polymer and materials science) to phase separation and porosity. At these larger size-scales, the technique is insensitive to atomic separation in materials, but rather the arrangement of assemblies of atoms enables molecular structures

and their spatial distribution to be determined. As a consequence, small-angle scattering, either with X-rays (SAXS) or neutrons (SANS) has been widely applied to food-based systems. The theory of small-angle X-ray and neutron scattering may be found in a wide range of texts (Jacrot, 1976; Feigin & Svergun, 1987; Guinier & Fournet, 1955; Glatter & Kratky, 1982; King, 1999; Wignall, 1993; Lindner & Zemb, 1991; Hammouda, 2008). For structural information on even larger scales, ultra small-angle scattering (USANS/USAXS) can be applied up to tens of microns (Figure 3.1). These methods are outside the scope of this chapter however. Opportunities also exist to measure SAXS and XRD simultaneously (Loisel, 1998) as well as with differential scanning calorimetry (Vermeylen et al., 2006; Gilbert et al., 2005).

A small-angle scattering experiment conventionally measures the intensity of scattered radiation versus q where q is the scattering vector. q is defined to be equal to $(4\pi/\lambda)\sin\theta$, and, as per XRD, 2θ is the scattering angle and λ is the wavelength of the incident radiation. For isotropic scatterers, the data are typically radially averaged to give the scalar quantity q.

The measured intensity in a SAS experiment may be written:

$$I(q) = \frac{d\Sigma}{d\Omega}(q) = (\Delta\rho)^2 V_p^2 N_P P(q) S(q) \tag{3.1}$$

where $d\Sigma/d\Omega(q)$ is the differential scattering cross-section, $\Delta\rho$ is the scattering contrast between the species of interest and its surroundings (defined below), V_p is the volume of the species, N_p is the number of species per unit volume, P(q) is the form factor and S(q) is the structure factor. $d\Sigma/d\Omega(q)$ contains all the information regarding the size, shape and interactions between the scattering species in the sample. P(q) describes the scattering from an individual scattering species whereas S(q) describes the scattering between scattering centres. In other words, P(q) represents an intraparticle property whereas S(q) represents an interparticle property.

For small-angle scattering to be observed, there must be a contrast in scattering between the system of interest and its surroundings; for example, between a protein and its surrounding solution. The scattering contrast, $\Delta\rho$, is equal to $\Delta\rho = \rho_p - \rho_{sm}$ where ρ_p and ρ_{sm} refer to the scattering length densities of the species of interest and solution or surrounding matrix, respectively. The scattering intensity is proportional to $(\Delta\rho)^2$.

The scattering length density, ρ, of a molecule with i atoms is defined as $\delta N_A \Sigma bi/M$ where δ is the bulk physical density of the molecule, N_A is Avogadro's number, bi is the scattering length of the ith atom in the molecule and M is the molecular weight. The contrast may thus be simply calculated from knowledge of the physical density of the molecule and its atomic composition. Neutron and X-ray scattering lengths for biologically-relevant elements are summarised in Table 3.1. Typical scattering length densities are expressed in units of $10^{-6}A^{-2}$ or $10^{10}cm^{-2}$.

For SAXS, the scattering length is determined by the electronic structure of the target atom. Since the number of protons in an atom is equal to the number of electrons, the X-ray scattering intensity increases linearly with atomic number. Consequently, it is the heavier elements in a material that will dominate the signal in X-ray scattering. While the number of protons in an atomic nucleus defines the elemental type, it is the number of neutrons that defines the elemental isotope. Neutrons are scattered by the atomic nucleus; this means that the scattering from different isotopes can differ significantly. The classic example of this isotopic dependence is the difference between hydrogen (one proton in nucleus) and its heavier isotope, deuterium (one proton and one neutron). In this case, the extent of neutron scattering, defined by a length whose magnitude effectively defines the size of the nucleus,

Table 3.1 Neutron and X-ray scattering lengths for biologically-relevant elements.

Atom	Nucleus	bcoh (10^{-12}cm)	bx-ray (10^{-12}cm)
Hydrogen	1H	–0.374	0.28
Deuterium	2H	0.667	0.28
Carbon	12C	0.665	1.69
Nitrogen	14C	0.940	1.97
Oxygen	16C	0.580	2.25
Phosphorus	31P	0.517	4.22
Sulphur	*32S	0.285	4.51

*Natural abundance 95%.

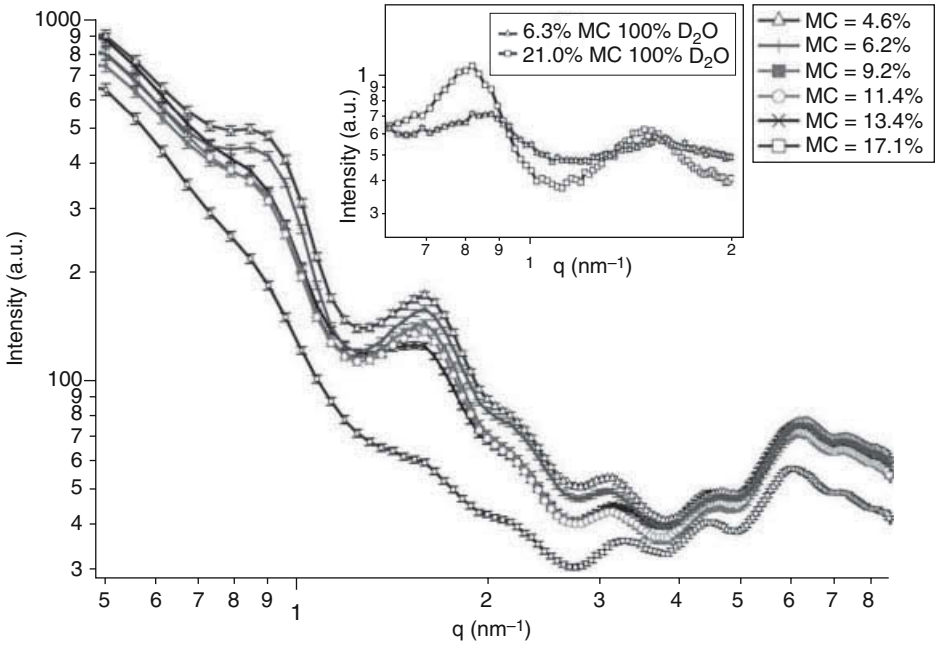

Figure 3.13 Small-angle X-ray scattering data from glycinin with increasing moisture content. The inset is a selected region from the small-angle neutron scattering data with H_2O replaced by D_2O at two moisture contents.
Source: from Kealley, C.S. et al., *J. Appl. Crystallogr.* 41, 628–633, 2008. International Union of Crystallography with permission http://journals.iucr.org.

is -0.3742×10^{-12}cm for hydrogen and 0.6671×10^{-12}cm for deuterium (Table 3.1); this length also represents the spatial extent of a pseudo-potential, thus the negative sign for hydrogen is associated with an effective attractive potential. This particular difference in scattering length between hydrogen and deuterium is extremely valuable for the study of hydrogen-containing materials and forms the basis of a method known as contrast variation discussed below.

Figure 3.13 shows the small-angle scattering from a powder of glycinin over a broad range of moisture contents (Kealley et al., 2008). Glycinin is a protein that accounts for 40% of the

total seed protein in soybean. Five major subunits of glycinin have been identified – A1aB1b, A2B1a, A1bB2, A3B4 and A5A4B3 (Utsumi et al., 1997; Adachi et al., 2001); however, crystal structures for only two of the five have been reported. Adachi et al. (2003) isolated the A3B4 subunit and reported a crystal structure for a homohexameric structure and determined that three hexamers are present in the hexagonal unit cell with dimensions of $a=b=11.484$, $c=19.157$ nm, and a volume of 2188 nm^3. This hexameric protein has a molecular mass of 300–380 kDa (Adachi et al., 2001) and each subunit is composed of an acidic (≈32 kDa) and a basic (≈20 kDa) polypeptide linked by a disulfide bond (Staswick et al., 1984).

The presence of peaks in the scattering is consistent with some degree of long-range order in the material with each peak position in q being related to a corresponding real-space dimension, $d=2\pi/q$. This example therefore demonstrates an example of X-ray diffraction, discussed above, but at small angles. Kealley et al. related the peak positions in this native material of unknown sub-unit composition to the single sub-unit Adachi structure showing it to be consistent with a hexagonal unit cell but with slightly smaller volume. Increasing moisture content was shown to result in an increase in this cell volume but with a corresponding decrease in scattering intensity; the latter is due to a decrease in scattering contrast between the protein and its surroundings. The concept of contrast is discussed in more detail below.

Although small-angle scattering may be used to investigate large unit cell crystalline materials, this is by no means the major application. The electrons (for X-rays) or nuclei (for SANS) in non-crystalline materials also give rise to scattering despite their atomic positions being less defined that those of crystalline materials. Indeed, it is possible to study the molecular structure of individual glycinin molecules from the small-angle scattering from solution (Figure 3.14). Here, data are collected at concentrations of 1 – 3 mg/mL as a function of pH and salt and where the influence of intermolecular interactions, i.e., S(q), may be neglected. In this case, the scattering intensity is proportional to the form factor related to the size and shape of the individual molecules and the difference in scattering density with respect to the surrounding medium, namely water, according to equation 3.1 above. Although S(q) can be treated as being equal to unity in the case of dilute solutions, this is certainly not the case in the powder state where S(q) effects gives rise to diffraction peaks as observed in Figure 3.13. Oscillations can be seen in the scattering from some of the samples that arise from the well-defined globular shape of the protein. Extreme acidic (pH2) and basic (pH11) environments, however, lead to the partial denaturation of glycinin; the associated broad distribution in protein morphologies results in a far less structured SAXS signal.

Several parameters may be extracted from the solution SAXS data. If a known standard sample is also measured so that the data are collected on an absolute scale and the concentration is known accurately then it is possible to determine the molecular weight of the particle. The application of Guinier's law enables the spatial extent of the scattering particle or radius of gyration, R_g, to be obtained from a plot of the logarithm of intensity against q^2. This parameter is related to the hydrodynamic radius measured in dynamic light scattering. R_g is a single parameter that represents the size of the scattering object. Its interpretation is simple in the case of a spherical scattering particle ($R_g=\sqrt{(3/5)}R$ where R is the radius of the object) but for non-spherical objects, R_g contains contributions from the other axes.

As the concentration of scattering objects increases in a system, interparticle effects start to become apparent and must be specifically considered. In this case, scattering can provide information concerning interparticle correlations and potential. One cannot define

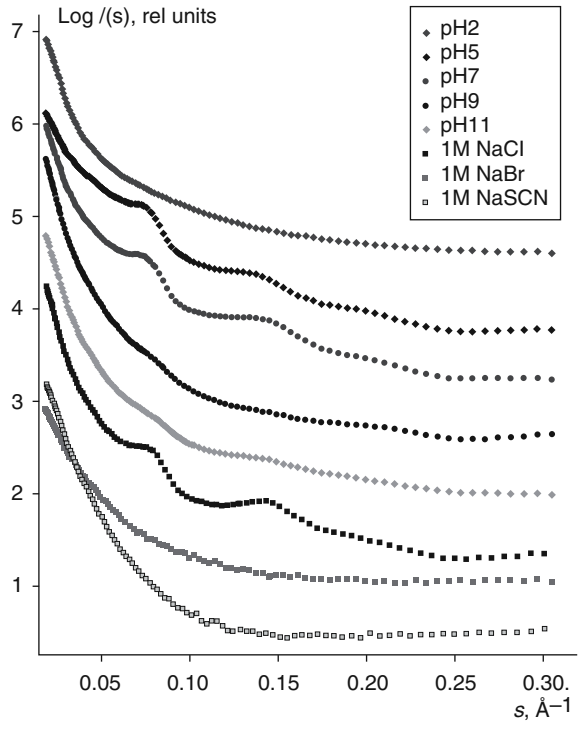

Figure 3.14 SAXS from solutions of glycinin as a function of pH and in the presence of 1 M salt. *Source*: from Sokolova et al., 2010, with permission, the American Chemical Society.

a concentration below which such effects may be neglected since these are an intrinsic property of the system. Clearly the influence of interparticle effects will become evident at significant lower concentrations in systems in which a Coulombic interaction between scattering objects takes place compared to uncharged particles. In practice, a concentration series is usually conducted in which the scattering as a function of concentration is compared. If no interparticle effects exist then the scattering between different concentrations should scale according to the concentration. The most concentrated system, with the absence of such effects, usually forms the basis for subsequent experiments. Interparticle interactions may present themselves either in the form of a reduction (repulsive interaction) or increase (attractive interaction, possibly leading to aggregation) and often in the low q region of the scattering patterns. In the extreme case, it would be evident as peaks in the scattering representative of some preferred separation between scattering objects which is analogous to characteristic repeat in a crystal.

There are several further parameters that may be obtained relatively simply via basic plots; R_g has been discussed above. If the scattering objects have one or more dimensions that are large compared to the inverse q values measured then characteristic slopes may be observable on log-log plots. For example, rod-like objects exhibit q^{-1} power law behaviour, disk-like objects show q^{-2} behaviour and objects with smooth-sharp interfaces exhibit q^{-4} behaviour. From the latter, surface area information may be obtained. Slopes between −3 and −4 characterise rough interfaces of a fractal dimension D with n=6-D. This is called a surface fractal. In the case of polymer coils, the Porod slope is the inverse of the excluded volume parameter ν. A slope of −2 is a signature of Gaussian chains in a dilute environment whereas

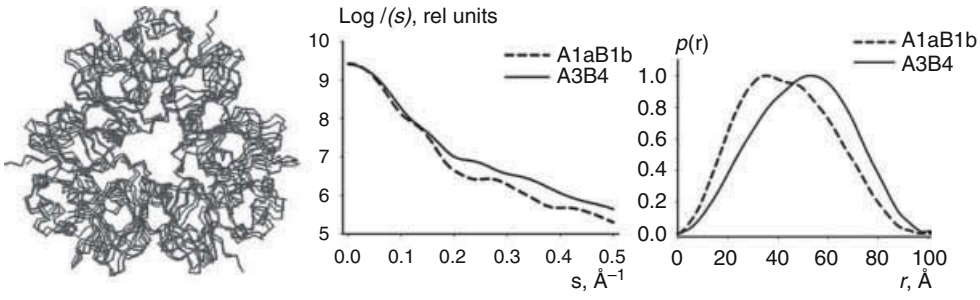

Figure 3.15 Trimers A1aB1b (red) and A3B4 (green) and corresponding calculated scattering intensities (middle panel) and p(r) functions (right panel).
Source: from Sokolova et al., 2010, with permission, the American Chemical Society.

a slope n=5/3 is observed for fully swollen coils and a slope of −3 for collapsed polymer coils. A slope between −2 and −3 is characteristic of 'mass fractals' such as branched systems (gels) or networks.

In the case of the glycinin powders above, the scattering arises from a combination of Bragg diffraction from the glycinin crystal structure and the interface between the protein and the surrounding medium. The latter is responsible for the intense scattering in the low-q region (also known as Porod scattering). Studies extending into the lower q range using USAXS indicates that the interface between the protein and the surrounding medium at a length-scale of at least 3 µm down to approximately 20 nm is smooth and sharp (Kealley et al., 2008). In situations in which the local environment causes aggregation to occur, the slope may also have a characteristic slope (Sokolova et al., 2010). Zimm plots may be used to determine the molecular weight, the radius of gyration and the second virial coefficient while Kratky plots illustrate the extent of deviation from Gaussian behaviour. The reader is invited to refer to the variety of books and reviews described above for further details on these approaches and the richness of information that may be obtained.

While these plots provide valuable information, their application may be limited by the complexity of the system under study. Scattering measurements are performed in Fourier (also called reciprocal) space and not in real space like microscopy. To obtain more detailed structural information, scattering data have to be either inverted back to real space – requiring data to be measured over a sufficiently broad q range to avoid truncation errors – or, alternatively, for models of the structure of the scattering system to be developed and then inverted and compared with experiment. For example, if data are collected over a sufficiently wide q range in the dilute regime (i.e., in the absence of interparticle effects) then the data can be Fourier transformed to generate a distance distribution function, P(r). This provides information not only on the spatial extent of the particle but also its shape. The P(r) function for the trimeric forms of glycinin composed of two different sub-units is shown in Figure 3.15 (Sokolova et al., 2010). If the protein being investigated has a reported crystal structure, more detailed information may be obtained. Further discussion of data analytical approaches specific to proteins, including *ab initio* methods and dummy atom modelling, are described in Svergun and Koch and references therein (2002; 2003).

The alternative is to generate a model that represents a hypothesis of the true structure of the scattering system. These models are Fourier transformed, compared with the experimental data and the model subsequently refined iteratively. Since there are a semi-infinite

number of possible mathematical solutions to such an inversion problem, it is essential that such models are based upon as much physical and chemical knowledge of the system as possible. It is often therefore valuable to utilise complementary imaging techniques such as transmission and scanning electron microscopy (TEM and SEM). In many cases, however, small-angle scattering is the only suitable technique capable of providing structural information without destroying the very region of the material that is of interest and whether the medium is a matrix, a solution or there exists one or more components in a mixture.

A classic example of the combination of SAXS and electron microscopy can be found in the study of complex macromolecular assemblies of native unfolded proteins and colloidal calcium phosphate, namely casein micelles. Despite widespread structural investigations, their structure remains a subject of debate. Two models have been proposed in which the casein micelles are either assumed to be composed of smaller protein-based submicelles linked via colloidal calcium phosphate (the submicelle model) or nanoclusters of colloidal calcium phosphate randomly distributed in a casein matrix (the nanocluster model). Both models possess a hairy layer in which the C-terminal end of κ-casein extends from the micelle surface and prevents flocculation via steric and electrostatic repulsion (Marchin et al., 2007). Note that the broad size range of casein micelles from 20 to 600 nm complicates the interpretation of the scattering and the larger sized micelles benefit from study by USAXS. Marchin et al. investigated the structure of casein micelles as a function of fractionation via centrifugation and found variations as a function of size with evidence pointing to the nanocluster model. More recently, Shukla et al. decorated casein micelles with tannins (2009) and were able to model their data using a polydisperse core-shell model consistent with calcium phosphate nanoclusters. These studies were extended more recently by Mata et al. to investigate milk protein concentrate powders, their individual components and associated solutions (Mata et al., 2011).

Microemulsions, comprising surfactant, oil and water have enormous potential in the development of functional foods taking advantage of their self-assembled microstructure, richness in morphology and thermodynamic stability (de Campo et al., 2004). Another attractive aspect is their ability to solubilise large amounts of lipophilic and hydrophilic food additives. The evolution of the microemulsion structure as a function of surfactant concentration or ingredient loading can be followed by scattering (Dave et al., 2007). For instance, it was observed that addition of salts in surfactant micellar solutions leads to the formation of more than one type of micelle (Aswal, 2003). De Campo et al. investigated the internal structure of aqueous submicron-sized dispersions of the binary monolinolein/water system, stabilised by a polymer, and demonstrated that the internal structure of the dispersed particles can be reversibly tuned by temperature (de Campo, 2004). Upon increasing the temperature, the internal structure undergoes a transition from cubic via hexagonal to fluid isotropic and vice versa.

Related to the above, controlled release has been widely exploited within the drug industry but much less so by the food industry (Bunjes & Unruh, 2007). This is likely to be an area of significant growth in food science due to the emerging success of functional foods (Sagalowicz, Leser, Watzke & Michel, 2006). Protection is needed for many bioactives as they are generally unstable and interact with oxygen or with other food components in the food matrix. For delivery systems, detailed characterisation is a major part of the research and development work to ensure the generation of systems with desirable properties. Proteins, lipids and carbohydrates can be used as matrices for encapsulation and controlled release (Ubbink & Kruger, 2006). For example, Fatouros et al. monitored the

in vitro digestion of a lipid-based formulation composed of oil, ethanol and surfactant using SAXS that spontaneously forms nanometres-sized oil droplets in an aqueous medium. The lipolysis could be followed in real-time, with a lamellar liquid crystal phase appearing immediately after initiation and a hexagonal phase being formed after one hour. This process is driven by lipase which continuously hydrolyses triglycerides from the oil cores of the nanoemulsion droplets into mono- and diglycerides and fatty acids (Fatouros et al., 2007). SAXS has been used to investigate edible oil organogels and fat crystal networks (Bot et al., 2008), creaming in tea (Jöbst et al., 2009) and the formation of agarose gels (Djabourov et al., 1989) where it has been demonstrated that size and shape information as well as interparticle distances can be measured.

The same information may be obtained from the small-angle scattering with neutrons (SANS) but neutron scattering provides several complementarities to SAXS (Lopez-Rubio and Gilbert, 2009). Contrast is a property that may be controlled via a method known as contrast variation (or contrast matching). For neutron scattering this relies on the different scattering lengths of hydrogen and deuterium. This means that molecules containing hydrogen may have their scattering length density varied by replacement with deuterium. The scattering length density for H_2O is negative ($-0.56\times10^{10}\,cm^{-2}$) and that of D_2O is positive ($6.38\times10^{10}\,cm^{-2}$). Thus, through the preparation of mixtures of H_2O and D_2O, particular components may be strategically contrast matched so that they effectively become transparent to neutrons. In a three component system, for example, two proteins that form a complex in solution, there may be occasion in which it is desirable to 'contrast match' out the contributions from one of the components; for example, to assess the conformational state of one protein within the complex.

Figure 3.16 shows the scattering length density for water and various biological macromolecules as a function of the deuterium concentration (Hammouda, 2008, adapted from Jacrot, 1976). The range of scattering length density that may be achieved through merely mixing normal and heavy water means that a selected biological component in a multi-component system can be contrast matched so that it has no contribution to the overall scattering. In the case of core-shell assemblies of nanoparticles, if the cores are selectively deuterated, then it is possible to make them transparent to neutrons by adjusting the scattering length density of the aqueous dispersion medium through its H_2O to D_2O ratio. This is shown schematically in Figure 3.17 and is equally possible for non-polar solvents using, for example, normal and deuterated forms of hexadecane (e.g. Reynolds et al., 2001). Parameters such as the thickness of the core and shell or the homogeneity of the internal structure can be extracted by fitting the SANS data to a core-shell model. Contrast variation may be achieved based on inherent differences in scattering as a result of chemical composition (as shown in Figure 3.16) or arise from strategic selective deuteration, e.g., replacement of hydrogen with deuterium in a fatty acid. It is worthy of note that the solvent scattering may be modified in X-ray scattering by the addition of various contrasting agents such as sucrose, glycerol or salts. For example, proteins may be contrast matched in 65% sucrose solutions (Svergun & Koch, 2003).

Due to the highly penetrating nature of neutrons, SANS offers a number of attractive opportunities. The technique provides bulk information with the scattering representative of the whole sample (as compared, for example, to scanning electron microscopy where only local information is obtained). It can also be applied to study materials contained within thick and complicated sample environments so that one may measure the structural changes of a material during a process. Thus a scattering measurement can be conducted in real-time of a complex fluid under shear in which the shear viscosity is measured simultaneously. In this way, the viscosity – a bulk property – may be related to the structure and orientation

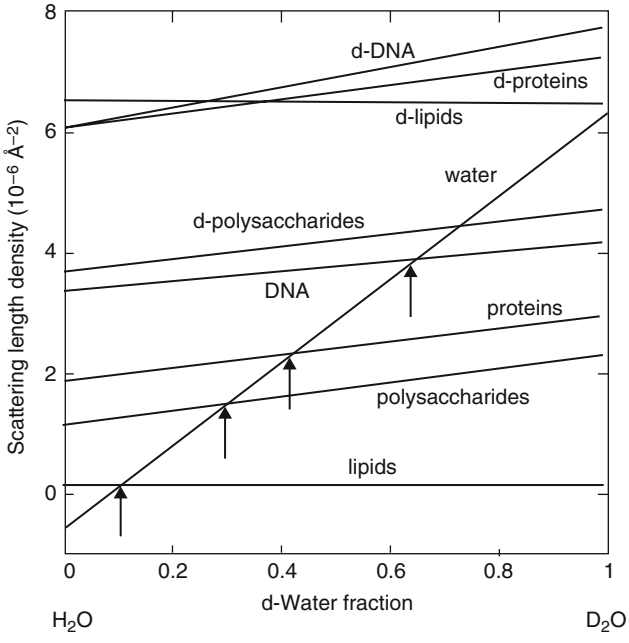

Figure 3.16 Neutron scattering length densities for common food-based materials.
Source: Lopez-Rubio and Gilbert (2009). Reprinted from *Trends in Food Science and Technology* 20, Neutron Scattering: A Natural Tool for Food Science and Technology Research, 576–586. Copyright (2009), with permission from Elsevier (after Hammouda, 2008; adapted from Jacrot, 1976).

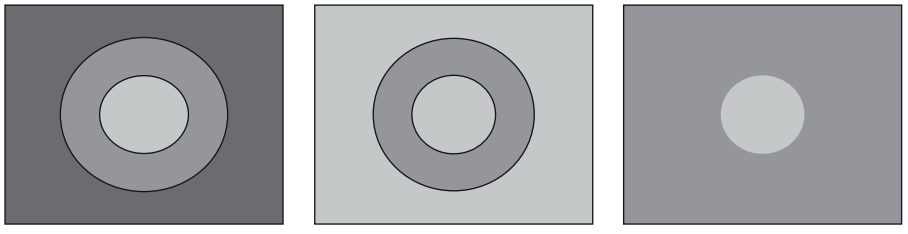

Figure 3.17 Core-shell nanostructure in solution showing the possibility of selectively contrast matching either of the phases through changing solvent H_2O/D_2O composition.
Source: Lopez-Rubio and Gilbert (2009). Reprinted from *Trends in Food Science and Technology* 20, Neutron Scattering: A Natural Tool for Food Science and Technology Research, 576–586, Copyright (2009), with permission from Elsevier.

of network strands – a molecular property (Förster, Konrad & Lindner, 2005). Herle, Kohlbrecher, Pfister, Fischer and Windhab have used this so-called rheo-SANS set-up to investigate vorticity bands in a worm-like micelle solution (Herle et al., 2007). Doutch et al. have recently studied a range of starches undergoing Rapid Visco Analysis while simultaneously measuring SANS to correlate structure with viscosity changes during a model cooking process (Doutch et al., 2012).

Starch granules are semicrystalline structures containing a lamellar arrangement of the two main constituent biopolymers (amylose and amylopectin). As a consequence, SAXS patterns from hydrated native starches show a broad scattering peak, from which the average

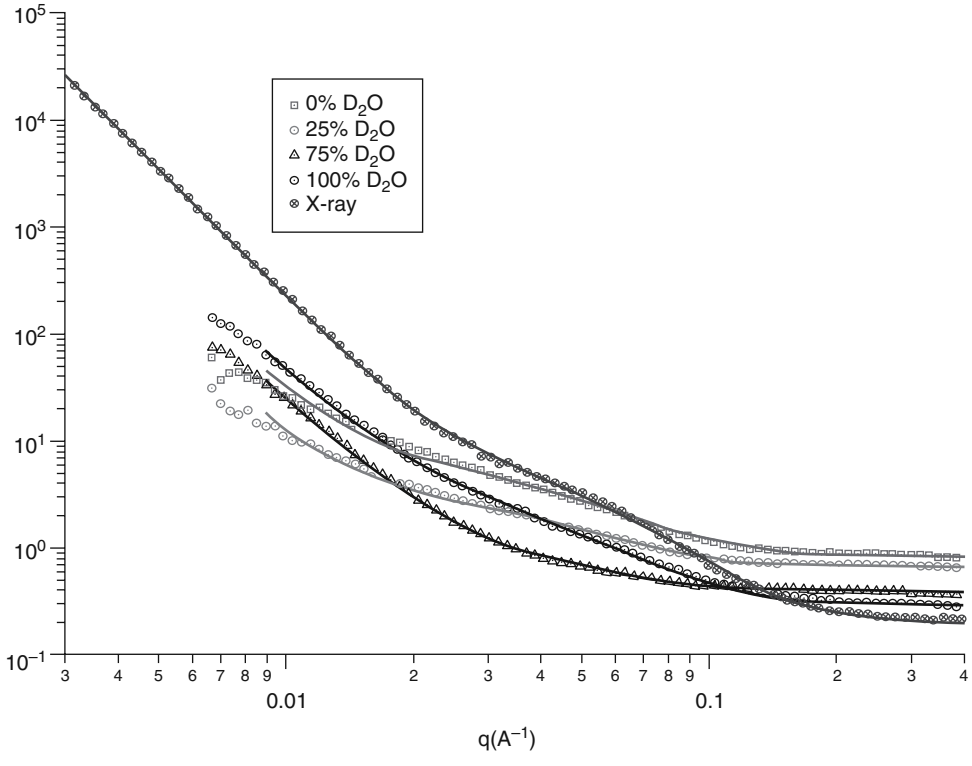

Figure 3.18 SANS patterns of resistant starch formed from processed high-amylose maize starch in water. Four neutron solvent contrasts have been used: 0% D_2O, (i.e. 100% H_2O), 25% D_2O:75% H_2O, 75% D_2O:25% H_2O and 100% D_2O along with an effective fifth contrast from SAXS. Dot points represent the experimental data that have been simultaneously fitted with a power law and two phase non-particulate model (solid lines).
Source: Lopez-Rubio and Gilbert (2009). Reprinted from *Trends in Food Science and Technology* 20, Neutron Scattering: A Natural Tool for Food Science and Technology Research, 576–586, Copyright (2009), with permission from Elsevier.

thickness of the lamellar repeat unit (crystalline plus amorphous region) may be calculated (Jenkins & Donald, 1996). In the absence of water, no such peak is observable. It has been implicated that this is a combination of a contrast effect, in which water is preferentially located within the amorphous regions of the lamella, and water enabling an increased mobility in the polymer chains so that a more ordered lamellar structure can be achieved. Complementary to SAXS, SANS provides the ability to quantify the distribution of water within the granule so that comparisons can be made both between different species and processes. Donald and co-workers (2001) used SANS to assess the validity of cluster model for the starch structure – consisting of three regions, i.e., semicrystalline stacks containing alternating crystalline and amorphous lamellae, embedded in a matrix of amorphous material – and to follow the gelatinisation behaviour of a range of starches allowing the location of water during the swelling of the granule before the melting transition of the materials (Jenkins & Donald, 1998) to be determined. Blazek and Gilbert recently investigated in-situ enzymatic digestion of a series of commercial granular starches (Blazek & Gilbert, 2010).

Resistant starch (RS) is a fraction of starch that is not digested in the small intestine of healthy individuals and arrives in the colon where a proportion is fermented into short-chain fatty acids. The latter molecules are beneficial for the correct functioning of the bowel and implicated in disease prevention (Topping & Clifton, 2001). Figure 3.18 shows the neutron patterns obtained at four different solvent conditions (varying the amount of D_2O/H_2O), together with the SAXS from a processed high amylose starch after 18 h of in vitro digestion.

The five scattering patterns have been simultaneously fitted to a six parameter model, including a power law describing the low q region and a term describing a two phase non-particulate system that has previously been observed to properly describe the scattering pattern of resistant starch (Lopez-Rubio, Htoon and Gilbert, 2007). The latter term incorporates parameters that yield the degree of crystallinity, the characteristic dimension and the scattering contrast between the crystalline and amorphous phases. From the fits, it was possible to determine that the contrast match point occurs for a solvent containing 58.6% D_2O, a value very similar to that of granular starch (Jenkins et al., 1996).

Contrast variation has been applied to study casein micelles since calcium phosphate and casein components have different neutron scattering length densities. This enabled Holt et al. (Holt et al., 1998; Holt et al., 2003) to develop the casein micelle nanocluster model. SANS has also been used to shed light on the physiology of lipid solubilisation in bile and on the digestion process of the bile-emulsified oil droplets (Lopez, Samseth, Mortensen, Rosenqvist & Rouch, 1996; Pignol et al., 2000). The morphologies of various conjugated bile salt-lipid systems have been extensively studied by Hjelm et al. who found sufficient similarities to suggest a common mode of self-assembly (Hjelm, Schteingart, Hofmann & Thiyagarajan, 2000). The broad application of small-angle neutron scattering to food-relevant systems is discussed in the review by Lopez-Rubio and Gilbert (2009) while examples on the application of both X-ray and neutron scattering specifically to starch may be found in Blazek and Gilbert (2011).

3.6 CONFOCAL MICROSCOPY

The objective of microscopy studies in food science has been to gain a thorough knowledge of the structural organisation of the main components of food materials and their relation to bulk properties, such as texture, stability and appearance. In this sense, confocal microscopy has provided a major advance in microscopy, constituting a bridge between conventional light microscopy with its limited resolution (but capable of imaging hydrated samples) on one side, and electron microscopy, with its higher resolution but far more involved sample preparation processes and limitations on the other. Confocal microscopy now offers not only an effective increase in imaging capabilities but also (when coupled to a computer/image processing system) vastly increased possibilities for specimen analysis and presentation (Brakenhoff et al., 1988).

Confocal microscopy is an optical imaging technique used to increase micrograph contrast and/or to reconstruct three-dimensional images by using a spatial pinhole to eliminate out-of-focus light in specimens that are thicker than the focal plane (Pawley, 2006). This is undoubtedly the major advantage of confocal microscopy when compared to traditional optical microscopy. An aspect implicit in the confocal principle, which deserves special attention is the sectioning property. In normal microscopy all the radiation generated at the various levels in the specimen reaches the image plane, causing a reduction of the contrast of the image of the in-focus part of the specimen. In confocal microscopy,

the detection pinhole used, together with the effect of the illumination precisely focused on the specimen point imaged, will suppress quite effectively the out-of-focus contributions. Thus, an image is produced which is only related to the in-focus specimen plane (Brakenhoff et al., 1988). In practice, this means that the sample can be scanned at different depths to obtain a z-series or gallery of images. A stack of z-series can be subsequently reconstituted using computer software, where the 3-D image of the original structure can be rotated or sliced in any direction (Vodovotz et al., 1996). This allows a precise view of the spatial arrangements of structural elements in the food sample.

A further advantage of confocal microscopy is the possibility to follow in situ the evolution of the microstructure of food systems when changing the ambient conditions; this enables the study of the dynamics of, for example, phase separation, coalescence, aggregation, coagulation and solubilisation. Specially designed stages that allow heating, cooling or mixing of the sample, provide the possibility to simulate food processing under the microscope (Thorvaldsson et al., 1998).

In contrast to electron microscopy techniques, minimal sample preparation is required in confocal microscopy and visualisation of the sample occurs at ambient conditions, which allows the observation of specimens in the hydrated state. In some cases, a few preparatory steps are necessary for viewing a specimen. For instance, the component of interest in the sample may be labelled. Fluorescent dyes are labelling agents which contain excitable structures that emit fluorescence after illumination by light of a specific wavelength. Moreover, labelling with specific fluorescent dyes enables detection of specific components (Sheppard & Shotton, 1997). In addition, there are fluorescent compounds sensitive to pH, enabling pH gradients in a sample to be detected (Hassan et al., 1995) and fluorescent dyes for detecting lipid oxidation and antioxidant capacity in living cells (Drummen et al., 2002). The latter have been used to study the migration of oxidation in a semi-hard yellow cheese (Westermann et al., 2009). Possibly, the need for staining of most samples constitutes the major limitation of this microscopy technique, as all steps such as staining or quenching of autofluorescence, which have to be performed in liquids at room temperature, can result in artefacts like swelling and solubilisation of components. Moreover, many fluorochromes are sensitive to laser-illumination and can bleach within the time necessary for searching and acquiring an image (Dürrenberger et al., 2001).

Lasers are commonly used as light sources in confocal microscopes, providing the advantages of being monochromatic and tightly collimated coherent beams (Cox, 1999). However, if the composition of the sample is less well known, it is often useful to illuminate it with white light to provide a true-colour image. For detailed information on laser sources, fluorescent dyes for sample staining and the image processing capabilities of commercially available image analysis software, the reader is directed to specific books (Sheppard & Shotton, 1997; Pawley, 2006) and reviews (Blonk & Von Aalst, 1993; Vodovotz et al., 1996; Ferrando & Spiess, 2000) focussed on the technique.

3.6.1 Applications of confocal microscopy in food science

Confocal microscopy has been widely used in food science to characterise the microstructure of gels and emulsions. The structural organisation at the microscopic level of these multiphase materials, their formation during processing and the effect of this structure on their stability are important aspects which determine shelf-life and oral melt behaviour of many food systems (Ferrando & Spiess, 2000).

As an example, confocal microscopy has been used to visualise different types of phase behaviour of mixtures of gelatine and polysaccharides. The images of the phase

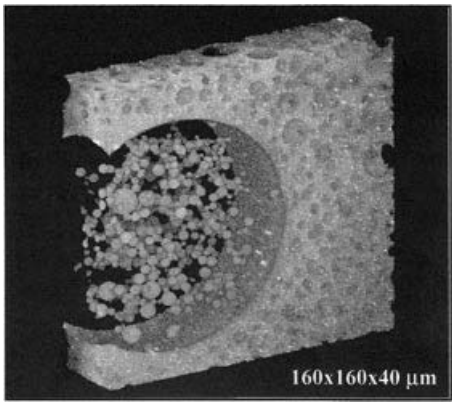

Figure 3.19 Phase separated gelatine/dextran/0.5 M NaCl. The dextran-rich phase is coloured. *Source*: Reprinted from *Food Research International* 34, Confocal scanning light microscopy (CSLM) on mixtures of gelatine and polysaccharides, 931–938, Copyright (2001), with permission from Elsevier.

separation between gelatine and dextran illustrate structure generation in food biopolymer mixtures. In particular, the 3D images show the effect of gelation of gelatine on liquid/liquid phase separation, which interestingly leads to what appears to be a 'double emulsion' of a dextran-rich phase in a gelatine-rich phase as shown in Figure 3.19. The most remarkable feature of this image, where the dextran phase is preferentially labelled, is the large open sphere with small spheres inside. The former is a gelatine-rich phase domain and the small spheres are dextran-rich inclusions. The small spheres were formed by the enhanced phase separation tendency during progressive gelation of the gelatine-rich domain. After their formation in the liquid state, gelatine-rich regions still contain dextran (Tromp et al., 2001).

Another interesting application of confocal microscopy is the visualisation of cheese structures in which fat droplets are embedded in the hydrated protein. Changes in the physicochemical properties and microstructure of the native milk fat globules may occur as a result of the treatments applied during processing. However, the structure of fat, its distribution and hence consequences on the textural, functional and sensory properties of dairy products are often unclear. Using confocal microscopy, the changes in the microstructure of milk fat globules during the manufacture and ripening stages of Emmental cheese were studied; it was found that pressing, identified as the main destabilising process, resulted in the greatest disruption of fat globules and plays a major role in the formation of free fat (Lopez et al., 2007). In another study, using differential staining, differences in the distribution of fat droplets and protein were studied in Gouda cheese, which are essential to understand the different texture and mouth feel of low fat and high fat cheeses (Heertje et al., 1987).

Pedreschi et al. (1999) developed a methodology for studying the oil location directly in fried potato chips with minimal intrusion using confocal microscopy. A thermoresistant fluorescent probe was used to stain the frying oil in which the potato samples were immersed. Observation of the different sample layers, followed by 3D reconstruction, proved that oil in the crust has an appearance of an 'egg-box' surrounding intact dehydrated potato cells but did not penetrate into them; this was later confirmed by Bouchon and Aguilera (2001).

3.7 SCANNING ELECTRON MICROSCOPY

Scanning electron microscopy (SEM) is an imaging technique used to characterise the morphology of sample surfaces by scanning them with a high-energy beam of electrons. The electrons interact with the atoms of the sample producing signals that contain information about the sample's surface topography. The types of signals produced include secondary electrons, backscattered electrons, characteristic X-rays and other photons of various energies. The imaging signals of greatest interest are the secondary and backscattered electrons because these vary primarily as a result of differences in surface topography (Goldstein et al., 2003).

Electrons are possibly the ideal excitation source for scanned probe microscopic imaging due to their intrinsic characteristics. Some features that make them attractive are (Pawley, 2008): (i) Mono-energetic sources of very high brightness are available; (ii) Their short wavelength, which coupled with available lenses, can provide very good focus characteristics; (iii) Due to the very narrow electron beam, SEM micrographs have a large depth of field yielding a characteristic three-dimensional appearance useful for understanding the surface structure of a sample; (iv) Electrons are charged, which makes it possible to use electromagnetic fields to scan the probe over the surface of the specimen rapidly and accurately; (v) Moreover, a wide range of magnifications is possible, from about 10 times (approximately equivalent to that of a powerful hand-lens) to more than half a million times, or about 250 times the magnification limit of the best light microscopes.

For conventional SEM, specimens must be electrically conductive, at least at the surface. In the food science area, where most of the materials are non-conductive, an ultrathin coating of electrically-conducting material, commonly gold, is required that is deposited on the sample either by low vacuum sputter coating or by high vacuum evaporation. Most food materials consist of carbon, hydrogen and oxygen, which are low atomic number elements. In these materials coating is important to maximise the signal and improve spatial resolution as, in general, signal increases with atomic number (Echlin, 2009). In a similar sense, this is the origin of the dominance of high atomic number elements in the signals obtained in SAXS and XRD.

Another important consideration is the susceptibility of food compounds to radiation damage; this results in limitations regarding the current intensity and the magnification that can be obtained. An inherent disadvantage of conventional SEM is that the equipment operates in vacuum. Therefore, a dehydration step is needed during sample preparation which can result in structure modification. This is especially important when trying to observe highly hydrated molecules such as polysaccharides (Hassan et al., 2003). To avoid morphological alterations as a consequence of dehydrating the samples, a common procedure is to fix the food specimens with glutaraldehyde in water or in a buffer, followed by a post-fixing method in a diluted solution of osmium tetroxide. Dehydration then takes place stepwise in increasing concentrations of ethanol and/or acetone. This traditional procedure has, for instance, enabled the observation of protein hydrolysates (Liu & Guo, 2008), bacterial biofilm formations on stainless steel (Rieu et al., 2008) and morphological alterations of caviar during storage (Gussoni et al., 2006). However, these sample preparation procedures are laborious and can also affect the morphology of the samples leading to artefacts. There are several possibilities to overcome this drawback, such as the immobilisation of the compounds in solid substrates, cryo-SEM and environmental or low pressure SEM (ESEM), which will be described together with some selected examples below.

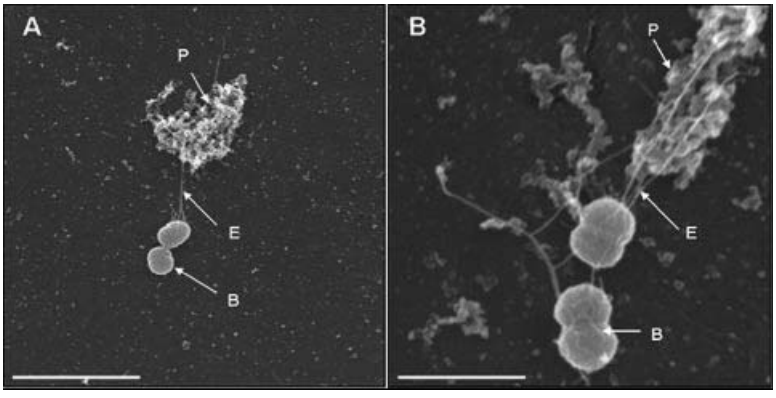

Figure 3.20 Scanning electron microscopy images obtained from a milk product fermented at pH 5.8. Panel A scale bar=3,000 nm; panel B scale bar=1,200 nm. E=exopolysaccharide; P=protein; B=bacterial cells.
Source: *Journal of Dairy Science* 91, Ayala-Hernandez, I., Goff, H.D., Corredig, M., Interactions between milk proteins and exopolysaccharides produced by *Lactococcus lactis* observed by scanning electron microscopy, 2583–2590, Copyright Elsevier (2008).

3.7.1 Immobilisation in solid substrates

SEM is a well-established technique often employed to observe the microstructure of dairy products; these are examples of highly hydrated systems. In fermented dairy products containing lactic acid bacteria, an increase in viscosity is usually observed, which has been ascribed to the production of exopolysaccharides (EPS) by bacteria. EPS are known to modify the texture, and increase the water holding capacity, in fermented dairy products. The observation of some milk biomolecules by electron microscopy techniques may be carried out after immobilisation to solid substrates. In this way it is possible to preferentially attach the molecules to be observed to the solid substrate and eliminate the remainder of the components by washing the sample holder. This approach has been used to observe the interactions between EPS produced by lactic acid bacteria and milk proteins (Ayala-Hernandez et al., 2008). From the micrographs obtained using the fixing technique, the strands of EPS emerging from the bacteria are seen embedded in the protein network (Figure 3.20) (Ayala-Hernandez, 2001). SEM of samples immobilised on self-assembled monolayers proved to be a valuable technique for the observation of EPS and their interactions with proteins. They also observed that the exopolysaccharides clearly interact, not only with caseins but also with whey proteins, and play an active role in the formation of aggregates. This may explain the viscosifying effect that the presence of EPS has in fermented dairy products.

3.7.2 Cryo-SEM

Conventional high-vacuum cryo-electron techniques for the study of fast-frozen hydrated specimens are well established and extremely useful for studying the 'static' microstructure of organic materials (Echlin, 1992). The greatest advantage of the cryo-SEM technique is that it enables the close examination of frozen liquids and very soft specimens. The technique involves fixing of the specimens by immersion in liquid nitrogen followed by sublimation

of water. As a result, cryo-SEM does not require chemical fixation or fat extraction, thus the examination of high moisture samples is made easier (Hassan et al., 2003).

This technique has been used to study the morphology of various cheeses. One of the trends in food science is to make low-fat versions of fermented milk products such as via partial replacement of fat with starch for the development of low-fat cheeses (Noronha et al., 2008). In this sense it is important to characterise the microstructure of the developed products as it significantly affects end-product processing characteristics (e.g., slicing, spreadability), flavour properties and texture. The high magnification of cryo-SEM has been useful in elucidating some features of the microstructure, particularly with respect to fat globules, such as their size and distribution. Micrographs show that starch type influences the microstructure of imitation cheese, in a way dependant on the properties of the starch, i.e., structure and gelatinisation temperature. For instance, pre-gelatinised starch, which has the ability to swell in cold water, competes with casein for the available water in the product thus limiting casein's hydration (Noronha et al., 2008).

3.7.3 Environmental SEM (ESEM)

The Environmental Scanning Electron Microscope (ESEM) is one of the latest developments in electron microscopy representing a major innovation and a great advance in the field. ESEM allows the examination of practically any specimen under any gaseous conditions, unlike conventional SEM which, as mentioned previously, operates in vacuum. This condition limits the SEM, since either the specimens have to be modified and compromised by various treatments or the microscope's operational parameters must be constrained. On the other hand, the ESEM enables soft, moist and/or electrically insulating materials to be viewed without pre-treatment and close to its natural state. A differential pumping system is used to maintain the electron gun at high vacuum, while the air at atmospheric pressure in the chamber is replaced by water vapour at low pressure (Goldstein et al., 2003). The low pressure inside the chamber limits the resolution of ESEM equipment to approximately 5 nm. However, the possibility of using different gas media allows for a number of options regarding operation and imaging (Stokes, 2003). Another major difference between SEM and ESEM is that samples do not need to be coated with a metallic layer before imaging. In ESEM, specimen temperatures and chamber pressures can be controlled independently. As food materials are sensitive to beam damage, low temperatures can be used to avoid, for instance, the melting of fats during observation. In addition, dynamic experiments can also be performed on ESEM equipment.

Such advantages have important implications in the food science area, as changes in the microstructure of the samples can be followed as a function of temperature and humidity. It is useful to store food ingredients in a dry state to keep them stable and handle them more easily. Rehydration of the ingredients will result in changes in morphology and thus properties. Therefore, the ability to study such changes as a function of water content is relevant to fulfil the needs of food manufacturers.

Morphological changes in glycinin were followed as a function of hydration/dehydration (Kealley et al., 2008). This is the protein discussed above and commonly used in foods as a gelling, emulsifying and foaming agent (Utsumi et al., 1997). The dry protein powders (4.6% moisture content) display a porous structure, with the porosity decreasing and microstructure

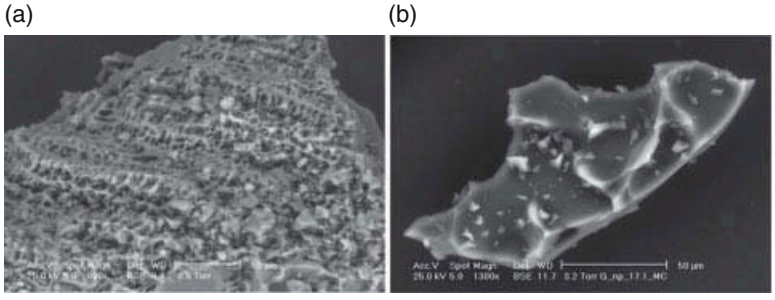

Figure 3.21 ESEM micrographs of (a) the 4.6% and (b) the 17.1% moisture content powder samples of glycinin.
Source: Kealley, C.S. et al., *J. Appl. Crystallogr.* 41, 628–33, 2008. International Union of Crystallography with permission.

expanding as the moisture content increases (final moisture content 17%) as shown in Figure 3.21. Decreasing the vapour pressure in the chamber, which causes a dehydration of glycinin, was seen to lead to shrinkage of the protein structure of about 20% (Kealley et al., 2008).

ESEM has also been used to shed some light on fat bloom formation in chocolate (Rousseau & Smith, 2008). Although it is known that fat bloom arises as a result of a polymorphic transition of the cocoa butter crystals, there is a lack of knowledge of a microstructure-based means of controlling it. Temperature-controlled ESEM was used to examine microstructural changes as a function of storage time in plain chocolate and in cream-filled chocolate. The formation of crystals during storage was significantly greater in the filled confectionary, and the crystals had different morphology. From the microstructural observations, it appears that diffusion and capillarity of liquid triglycerides affect fat bloom initiation and propagation, though temperature and the presence of a filling fat strongly dictate which mechanism will dominate (Rousseau & Smith, 2008).

3.8 ATOMIC FORCE MICROSCOPY (AFM)

Atomic Force Microscopy (AFM) relies on scanning a sharp probe, which is attached to a flexible cantilever, across a sample surface (Binning et al., 1986). It operates by measuring attractive or repulsive forces between the tip and the sample, which cause the cantilever to deflect. By monitoring the extent of cantilever bending as the cantilever-stylus assembly is scanned over the surface, any undulations in the sample can he recorded (Morris, 2004). The end result is a three dimensional profile of the surface under study.

The resolution that can be obtained is determined by the size and shape of the probe and by the accuracy with which it can be positioned relative to the sample surface. Under suitable conditions, atomic force microscopes are capable of imaging atoms and molecules. This offers the potential to characterise food materials that were previously difficult or even impossible to observe using other types of microscopies (Morris et al., 1999).

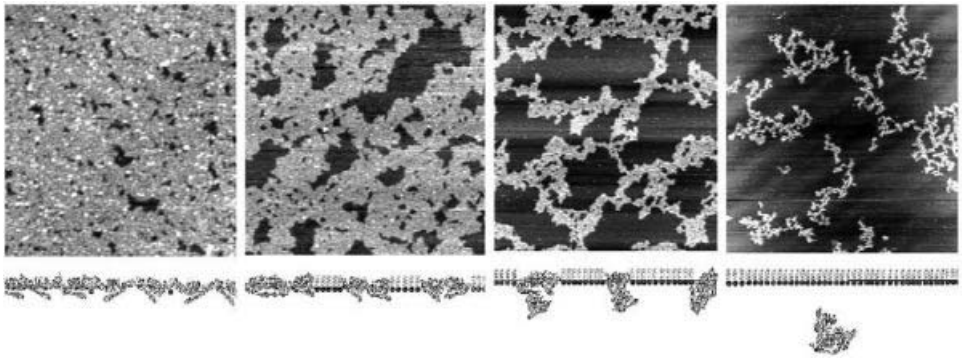

Figure 3.22 AFM images showing the displacement of a spread β-lactoglobulin protein film from an air-water interface by the progressive addition of the surfactant Tween 20. The image sizes are from left-to-right 1.0×1.0 mm, 1.6×1.6 mm, 3.2×3.2 mm and 10.0×10.0 mm. A schematic model of the displacement process is illustrated below the images.
Source: Reprinted from Morris 2004 with permission from Elsevier.

Different modes of AFM are available to emphasise molecular structure or to probe structural features such as charge or elasticity (Morris et al., 1999). A detailed description of the various associated analytical methods available as well as the most appropriate choice of operating mode - e.g. contact, non-contact or tapping, and either static or dynamic - can be found elsewhere (Wiesendanger, 1998; Bushan et al., 2004; Kaupp, 2006).

AFM has the advantage of imaging almost any type of surface, allowing biomolecules to be imaged not only under physiological conditions but also during biological processes. For instance, the mechanism by which surfactants displace proteins at interfaces has been studied 'in situ' within a liquid cell of AFM (Gunning et al., 1999). This mechanism is illustrated in Figure 3.22 and consists of an initial nucleation of the surfactant within defects in the protein network; this subsequently causes refolding of proteins and buckling of the protein network with the result that the protein escapes into the bulk phase. This mechanism has been shown to be generic for all the proteins and surfactants studied to date (Morris, 2004).

A further advantage of the technique is that sample preparation is simple and comparable to that employed in light microscopy. The only requisite is that the sample has to be immobilised onto a substrate, such as mica or glass, the roughness of which dictates the level of detail observable on the specimen (Morris et al., 1999). The important parameter to be determined to obtain a good level of contrast in the final image is the force that has to be exerted on the sample by the probe. If too low a force is applied, the probe 'mistracks' and the resultant contrast is poor, while if too high force is applied, this can cause distortions, damaging the sample surface or displacing the contents thereof (Morris et al., 1999).

AFM images provide information on the surface structure of biomolecular systems, which is complementary to other established techniques such as light and electron microscopy, nuclear magnetic resonance (NMR), and X-ray crystallography. In comparison with, for instance, X-ray diffraction, the detailed topological information is not restricted to highly ordered specimens due to the high signal-to-noise ratio of the technique. Hence, single biomolecules without inherent symmetry can be directly monitored in their native environment (Luykx et al., 2008). Gunning and co-workers (2003) imaged

single amylose molecules after depositing them onto a mica substrate. The images showed stiff extended helical molecules from which the molecular mass and polydispersity could be determined.

Due to the potential of the technique in the food science area, the number of studies in the field using this technique is slowly but consistently increasing. Some recent investigations on food systems using AFM are described below.

3.8.1 Applications of atomic force microscopy in food science

Polysaccharides and proteins are macromolecules widely used in food products to generate different textures. In concentrated solutions, the molecular chains of these biopolymers interpenetrate and form entangled networks. These three dimensional hydrated networks can form as food gels and are of tremendous technological importance. Considerable research efforts have gone into the production of molecular models of the gelation processes and AFM offers an opportunity for imaging hydrated gels at molecular resolution (Kirby et al., 1995).

Some interesting studies carried out on polysaccharide gels using AFM show that the understanding of the structure at the nanoscale can be used to predict the macromolecular behaviour (Funami et al., 2007 and 2009). Funami and coworkers studied the nanostructure of carrageenan (2007) and gellan aqueous gels (2009), correlating the results with their rheological properties. The authors used a number of sample preparation procedures to verify that the images they obtained were representative of the real state of the material.

AFM has also been used to gain a better insight into the starch granule architecture. For instance, the technique has been used to confirm the 'blocklet' structure proposed by Buléon and co-workers (1988), suggesting the presence of packets of crystalline amylopectin within the granule (Ridout et al., 2002). The size and structure of amylose complexes produced by different methods has also been studied using AFM (Lalush et al., 2005). In this study, the technique was helpful in elucidating the origin of differences in the functionality of the complexes.

Apart from the imaging capabilities, AFM can also be used as a measuring tool. The mechanical properties of the systems under study can be extracted from the force curves obtained. This possibility broadens the application of AFM, not only as an imaging technique, but also as a tool to correlate structure and functionality. AFM stiffness and elasticity measurements were used, for instance, to obtain a quantitative comparison of bacterial integrity after treatment with garlic extract, which is known to have antimicrobial properties (Perry et al., 2009). The results obtained gave insights into the mechanism of action of the product, highlighting that garlic compounds might have intracellular activity as, in contrast with other antimicrobial compounds, it does not alter the elasticity of the cells.

This measuring ability of AFM was also used to probe the adhesion forces between *Escherichia coli* and a model surface, determining the effect of cranberry products on such adhesion (Pinzón-Arango et al., 2009). Previous clinical research has suggested that the consumption of cranberry products prevents the adhesion of *Escherichia coli* to uroepithelial cells by causing changes in bacterial fimbriae. Using AFM, it was observed that growing the bacteria in broth supplemented with light cranberry juice or cranberry proanthocyanidins resulted in a decrease in adhesion forces. However, the effect was reversible and if the bacteria were re-grown in cranberry-free medium, they regained their ability to attach to uroepithelial cells with adhesion forces similar to those of the control. From the results obtained, the authors concluded that alteration of adhesion

forces and attachment of bacteria depends on the concentration of cranberry products and number of cultures exposed to them (Pinzón-Arango et al., 2009).

3.9 SUMMARY

To understand the relationship between the structure of food and its associated functional behaviour and properties requires a broad range of materials characterisation techniques. This is even more the case if some predictability of these factors is desired to enable the development of novel materials. The techniques selected in this chapter have been widely applied across a variety of food systems and enable study over a multitude of length scales. However, many more have been omitted such as dynamic and static light scattering, diffuse wave spectroscopy, differential scanning calorimetry, not to mention mechanical methods. Since the vast majority of food materials are multi-phase, multi-component and multiscale systems, the food materials scientist requires a broad arsenal of methods to enable their interrogation. Furthermore, since these materials are frequently characterised by kinetically-trapped, non-equilibrium states, characterisation must be conducted across broad time domains. As greater attention is awarded to real-time, perhaps in vivo studies, the interest in this rich field of science will only continue to grow and amaze.

REFERENCES

Adachi, M., Takenaka, Y., Gidamis, A.B., Mikamu, B. & Utsumi, S.J. (2001) Crystal structure of soybeam proglycinin A1aB1b homotrimer. *Molecular Biology*, 305, 291–305.

Adachi, M., Kanamori, J., Masuda, T., Yagasaki, K., Kitamura, K., Mikami, B. & Utsumi, S. (2003) Crystal structure of soybean 11S globulin: glycinin A3B4 homohexamer. *Proceedings of the National Academy of Science USA*, 100, 7395–7400.

Aguilera, J. & Lillford, P. (2008) *Food Materials Science*. Springer, New York.

Anastasiadi, M., Zira, A., Magiatis, P., Haroutounian, S.A., Skaltsounis, A.L. & Mikros, E. (2009) H-1 NMR-based metabonomics for the classification of Greek wines according to variety, region, and vintage. Comparison with HPLC data. *Journal of Agricultural Food Chemistry*, 57, 11067–74.

Aravind, N., Sissons, M., Fellows, C.M., Blazek, J. & Gilbert, E.P. (2012) Effect of inulin soluble dietary fibre addition on technological, sensory, and structural properties of durum wheat spaghetti, *Food Chemistry* 132, 993–1002.

Aswal, V.K. (2003) Salt effect in ionic mixed micelles. *Chemical Physics Letters*, 371, 371–7.

Atalla, R.H. & VanderHart, D.L. (1984) Native cellulose – a composite of 2 distinct crystalline forms. *Science*, 223, 283–5.

Atkins, P. & de Paula, J. (2002) *Physical Chemistry*, 7th Ed. Oxford University Press, Oxford, UK.

Ayala-Hernandez, I., Goff, H.D. & Corredig, M. (2008) Interactions between milk proteins and exopolysaccharides produced by *Lactococcus lactis* observed by scanning electron microscopy. *Journal of Dairy Science*, 91, 2583–90.

Belton, P. (ed) *The Chemical Physics of Food*. Blackwell Publishing Ltd., Oxford.

Binning, G., Quate, C.F. & Gerber, Ch. (1986) Atomic Force Microscope. *Physical Review Letters*, 56, 930–3.

Blazek, J. & Gilbert, E.P. (2010) The effect of enzymatic hydrolysis on native starch granule structure. *Biomacromolecules*, 11, 3275–89.

Blazek, J. & Gilbert, E.P. (2011) The Use of Scattering Techniques in Understanding Starch Structure: A Review. *Carbohydrate Polymers*, 85, 281–93.

Blonk, J.C.G. & van Aalst, H. (1993) Confocal scanning light microscopy in food research. *Food Research International*, 26, 297–311.

Bociek, S.M., Ablett, S. & Norton, I.T. (1985) A C-13-NMR study of the crystal polymorphism and internal mobilities of the triglygerides, tripalmitin and tristearin. *Journal of the American Oil Chemists' Society*, 62, 1261–6.

Bot, A., den Adel, R. & Roijers, E.C. (2008) Fibrils of γ-Oryzanol + β-Sitosterol in Edible Oil Organogels, *Journal of the American Oil Chemists' Society*, 85, 1127–34.

Bouchon, P. & Aguilera, J.M. (2001) Microstructural analysis of frying potatoes. *International Journal of Food Science and Technology*, 36, 669–76.

Brakenhoff, C.J., van der Voort, H.T.M., van Spronsen, E.A. & Nenninga, N. (1988) 3-dimensional imaging of biological structures by high resolution confocal scanning laser microscopy. *Scanning Microscopy*, 2, 33–40.

Brown, S.P. (2009) Recent advances in solid-state MAS NMR methodology for probing structure and dynamics in polymeric and supramolecular systems. *Macromolecular Rapid Communications*, 30, 688–716.

Buléon, A., Colonna, P., Planchot, V. & Ball, S. (1988) Starch granules: structure and biosynthesis. *International Journal of Biological Macromolecules*, 23, 85–112.

Buléon, A., Colonna, P., Planchot, V. & Ball, S. (1998a) Starch granules: structure and biosynthesis. *International Journal of Biological Macromolecules*, 23, 85–112.

Buléon, A., Gerard, C., Riekel, C., Vuong, R. & Chanzy, H. (1998b) Details of the Crystalline Ultrastructure of C-Starch Granules Revealed by Synchrotron Microfocus Mapping. *Macromolecules*, 31, 6605–10.

Bunjes, H. & Unruh, T. (2007) Characterization of lipid nanoparticles by differential scanning calorimetry, X-ray and neutron scattering. *Advanced Drug Delivery Reviews*, 59, 379–402.

Bushan, B., Fuchs, H. & Hosaka, S. (2004) *Applied Scanning Probe Methods*. Berlin, Springer.

de Campo, L., Yaghmur, A., Sagalowicz, L., Leser, M.E., Watzke, H. & Glatter, O. (2004) Reversible Phase Transitions in Emulsified Nanostructured Lipid Systems, *Langmuir*, 20, 5254–61.

Cava, D., Lagaron, J.M., Lopez-Rubio, A., Catala, R. & Gavara, R. (2004) On the applicability of FT-IR spectroscopy to test aroma transport properties in polymer films. *Polymer Testing*, 23, 551–7.

Cava, D., Catala, R., Gavara, R. & Lagaron, J.M. (2005) Testing limonene diffusion through food contact polyethylene by FT-IR spectroscopy: film thickness, permeant concentration and outer medium effects. *Polymer Testing*, 24, 483–9.

Chen, P. & Zhang, L. (2006) Interaction and properties of highly exfoliated soy protein/montmorillonite nanocomposites, *Biomacromolecules*, 7, 1700–06.

Cordella, C., Moussa, I., Martel, A.-C., Sbirrazzuoli, N. & Lizzani-Cuvelier, L. (2002) Recent developments in food characterization and adulteration detection: technique-oriented perspectives. *Journal of Agricultural and Food Chemistry*, 50, 1751–64.

Cox, G. (1999) Equipment for mass storing and processing of data. In: *Methods of Enzymology*, Volume 307: Confocal Microscopy (ed P.M. Conn), pp. 29–55. Academic Press, California, USA.

Crank, J. (1975) *The Mathematics of Diffusion*. Second Edition. Oxford Science Publications, Oxford (UK).

Cullity, B.D. (1956) *Elements of X-Ray Diffraction* (3rd Edition). Addison-Weesley, Reading, Massachusetts, United States.

Curley, D.M., Kumosinski, T.F., Unruh, J.J. & Farrell, H.M. (1998) Changes in the secondary structure of bovine casein by Fourier transform infrared spectroscopy: effects of calcium and temperature. *Journal of Dairy Science*, 81, 3154–62.

Dave, H., Gao, F., Schultz, M. & Co, C.C. (2007) Phase behavior and SANS investigations of edible sugar-limonene microemulsions. *Colloids and Surfaces A: Physicochemical and Engineering Aspects*, 296, 45–50.

Diez-Pena, E., Quijada-Garrido, I., Barrales-Rienda, J.M., Schnell, I. & Spiess, H.W. (2005) Advanced H-1 solid-state NMR spectroscopy on hydrogels, 1 – the effect of hydrogen bonding in the collapse of poly(methacrylic acid) hydrogels. *Macromolecular Chemistry and Physics*, 205, 430–7.

Donald, A.M., Kato, K.L., Perry, P.A. & Waigh, T. A. (2001) Scattering studies of the internal structure of starch granules. *Starch/Starke*, 53, 504–12.

Djabourov, M., Clark, A.H., Rowlands, D.W. & Ross-Murphy, S.B. (1989) Small-angle x-ray scattering characterization of agarose sols and gels, *Macromolecules*, 22, 180–8.

Drummen, G.P.C., van Liebergen, L.C.M., Op den Kamp, J.A.F. & Post, J.A. (2002) C_{11}-BODIPY581/591, an oxidation-sensitive fluorescent lipid peroxidation probe: (micro) Spectroscopic characterisation and validation of methodology. *Free Radical Biology and Medicine*, 33, 473–90.

Dürrenberger, M.B., Handschin, S., Conde-Petit, B. & Escher, F. (2001) Visualisation of food structure by confocal laser scanning microscopy (CLSM). *Lebensmittel-Wissenschaft und Technologie*, 34, 11–17.

Echlin, P. (1992) *Low-temperature microscopy and analysis*. Plenum Press, New York.
Echlin, P. (2009) *Handbook of sample preparation for scanning electron microscopy and X-Ray Microanalysis*. Springer, New York.
Fang, Y. & Dalgleish, D.G. (1997) Conformation of β-lactoglobulin studied by FT-IR: effect of pH, temperature and adsorption to the oil-water interface. *Journal of Colloid and Interface Science*, 196, 292–8.
Fang, Y. & Dalgleish, D.G. (1998) The conformation of α-lactalbumin as a function of pH, heat treatment and adsorption at hydrophobic surfaces studied by FT-IR. *Food Hydrocolloids*, 12, 121–6.
Fatouros, D.G., Roshan Deen, G., Arleth, L., Bergenstahl, B., Seier Nielsen, F., Skov Pedersen, J. & Mullertz, A. (2007) Structural Development of Self Nano Emulsifying Drug Delivery Systems (SNEDDS) During In Vitro Lipid Digestion Monitored by Small-angle X-ray Scattering, *Pharmaceutical Research*, 24, 1844–53.
Feigin, L.A. & Svergun, D.I. (1987) *Structure Analysis by Small-Angle X-Ray and Neutron Scattering*, Plenum Press, New York .
Ferrando, M. & Spiess, W.E.L. (2000) Review: confocal scanning laser microscopy. A powerful tool in food science. *Food Science and Technology International*, 6, 267–84.
Food Colloids Conference (2012) – Food Colloids – www.foodcolloids2012.life.ku.dk/
Förster, S., Konrad, M. & Lindner, P. (2005) Shear thinning and orientational ordering of wormlike micelles. *Physical Review Letters*, 94, 017803.
Foster, T.J., Ablett, S., McCann, M.C. & Gidley, M.J. (1996) Mobility – resolved 13C NMR spectroscopy of primary plant cell walls. *Biopolymers*, 39, 51–66.
Funami, T., Hiroe, M., Noda, S., Asai, I., Ikeda, S., & Nishinari, K. (2007) Influence of molecular structure imaged with atomic force microscopy on the rheological behavior of carrageenan aqueous systems in the presence or absence of cations. *Food Hydrocolloids*, 21, 617–29.
Funami, T., Noda, S., Nakauma, M., Ishihara, S., Takahashi, R., Al-Assaf, S., Ikeda, S., Nishinari, K. & Phillips, G.O. (2009) Molecular structures of gellan gum imaged with atomic force microscopy (AFM) in relation to the rheological behavior in aqueous systems in the presence of sodium chloride. *Food Hydrocolloids*, 23, 548–54.
Gidley, M.J. & Bociek, S.M. (1985) Molecular organisation in starches: a 13C CP/MAS NMR study. *Journal of the American Chemists' Society*, 107, 7040–4.
Gidley, M.J. (1992) High resolution solid state NMR of food materials. *Trends in Food Science and Technology*, 3, 231–6.
Gilbert, E.P., Nelson, A., Sutton, D., Terrill, N., Martin, C., Lal, J. & Lang, E. (2005) Phase Separation in the Organic Solid State: The Influence of Quenching Protocol in Unstable n-Alkane Blends, *Molecular Crystals & Liquid Crystals*, 440, 93–105.
Glatter, O. & Kratky, O. (1982) *Small Angle X-Ray Scattering*, Academic Press, London.
Gnanasambandam, R. & Proctor, A. (2000) Determination of pectin degree of esterification by diffuse reflectance Fourier transform infrared spectroscopy. *Food Chemistry*, 68, 327–32.
Goldstein, J., Newbury, D.E., Joy, D.C., Echlin, P., Lifshin, E., Sawyer, L. & Michael, J. (2003) *Scanning Electron Microscopy and X-Ray Microanalysis*. 3rd ed. Springer Science + Business Media, New York.
Guinier, A. & Fournet, G. (1955) *Small-Angle Scattering of X-Rays*. John Wiley & Sons, New York.
Gunning, A.P., Mackie, A.R., Wilde, P.J. & Morris, V.J. (1999) In-situ observation of surfactant-induced displacement of protein by atomic force microscopy. *Langmuir*, 15, 4636–40.
Gunning, A.P., Giardina, T.P., Faulds, C., Juge, N., Ring, S.G., Williamson, G. & Morris, V.J. (2003) Surfactant-mediated solubilisation of amylose and visualisation by atomic force microscopy. *Carbohydrate Polymers*, 51, 177–82.
Gussoni, M., Greco, F., Vezzoli, A., Paleari, M.A., Moretti, V.M., Beretta, G., Caprino, F., Lanza, B. & Zetta, L. (2006) Monitoring the effects of storage in caviar from farmed *Acipenser transmontanus* using chemical, SEM and NMR methods. *Journal of Agricultural and Food Chemistry*, 54, 6725–32.
Guthrie, S.E., Mazzanti, G. & Idziak, S.H.J. (2005) X-ray phase identification of chocolate is possible without the removal of sugar, *European Journal of Lipid Science Technology*, 107, 656–9.
Hambleton, A., Debeaufort, F., Beney, L., Karbowiak, T. & Voilley, A. (2008) Protection of active aroma compound against moisture and oxygen by encapsulation in biopolymeric emulsion-based edible films. *Biomacromolecules*, 9, 1058–63.
Hammouda, B. (2008) The SANS Toolbox. www.ncnr.nist.gov/staff/hammouda/the_SANS_toolbox.pdf.
Hassan, A.N., Frank, J.F., Farmer, M.A., Schmidt, K.A., Shalabi, S.I. (1995) Formation of yoghurt microstructure and three-dimensional visualisation as determined by confocal scanning laser microscopy. *Journal of Dairy Science* 78, 2629–2636.

Hassan, A.N., Frank, J.F. & Elsoda, M. (2003) Observation of bacterial exopolysaccharide in dairy products using cryo-scanning electron microscopy. *International Dairy Journal*, 13, 755–62.

Haque, K. & Roos, Y.H. (2005) Crystallisation and X-ray diffraction of crystals formed in water-plasticised amorphous spray-dried and freeze-dried lactose-protein mixtures. *Carbohydrate Research*, 340, 293–301.

Heertje, I., van der Vlist, P., Blonk, J.C.G., Hendrickx, H.A.C.M. & Brakenhoff, G.J. (1987) Confocal scanning laser microscopy in food research: some observations. *Food Microstructure*, 6, 115–120.

Herle, V., Kohlbrecher, J., Pfister, B., Fischer, P. & Windhab, E.J. (2007) Alternating vorticity bands in a solution of wormlike micelles, *Physical Review Letters*, 99, 158302.

Hjelm, R.P., Schteingart, C.D., Hofmann, A.F. & Thiyagarajan, P. (2000) Structure of conjugated bile salt fatty acid monoglyceride mixed colloids: studies by small-angle neutron scattering. *Journal Physical Chemistry B*, 104, 197–211.

Holt, C., de Kruif, C.G., Tuinier, R. & Timmins, P.A. (2003) Substructure of bovine casein micelles by small-angle X-ray and neutron scattering. *Colloids and Surfaces A: Physicochemical and Engineering Aspects*, 213, 275–84.

Holt, C., Timmins, P.A., Errington, N. & Leaver, J. (1998) A core shell model of calcium phosphate nanoclusters stabilized by β-casein phosphopeptides, derived from sedimentation equilibrium and small-angle X-ray and neutron-scattering measurements. *European Journal of Biochemistry*, 252, 73–8.

Huson, M., Strounina, E., Kealley, C.S., Rout, M.K., Church, J., Appelqvist, I.A.M., Gidley, M.J. and Gilbert, E.P. (2011) Effects of Thermal Denaturation on the Solid-State Structure and Molecular Mobility of Glycinin. *Biomacromolecules*, in press.

International Symposium on Food Rheology and Structure – www.isfrs.ethz.ch

Isiguro, T., Ono, T., Nakasoto, K. & Tsukamoto, C. (2005) Rapid measurement of phytate in soy products by mid-infrared spectroscopy. *Journal of Food Science*, 70, C63–C66.

Jacrot, B. (1976) The study of biological structures by neutron scattering from solution. *Reports on Progress in Physics*, 39, (10), 911–53.

James Doutch, Mark Bason, Ferdi Franceshcini, Kevin James, Douglas Clowes, Elliot P. Gilbert (2012) Structural Changes during Starch Pasting using Simultaneous Rapid Visco Analysis and Small-Angle Neutron Scattering, *Carbohydrate Polymers* 88, 1061–1071.

Jenkins, P.J. & Donald, A.M. (1996) Application of small-angle neutron scattering to the study of the structure of starch granules. *Polymer*, 37, 5559–68.

Jenkins, P.J., & Donald, A.M. (1998) Gelatinisation of starch – a combined WAXS/SAXS/DSC and SANS study. *Carbohydrate research*, 308, 133–47.

Jöbstl, E., Patrick, J., Fairclough, A., Davies, A.P. & Williamson, M.P. (2005) Creaming in Black Tea, *Journal of Agricultural Food Chemistry*, 53, 7997–8002.

Johns, M.L. & Hollingsworth, K.G. (2007) Characterisation of emulsion systems using NMR and MRI. *Progress in Nuclear Magnetic Resonance Spectroscopy*, 50, 51–70.

Johnson, J.L., Curtis Busk, G. & Labuza, T.P. (1980) Examination of the crystallinity of food gels by x-ray diffraction. *Journal of Food Science*, 45, 77–83.

Kaupp, G. (2006) *Atomic force microscopy, scanning nearfield optical microscopy and nanoscratching: application to rough and natural surfaces*. Berlin: Springer-Verlag.

Kealley, C.S., Elcombe, M.M., Wuhrer, R. & Gilbert, E.P. (2008) Application of small-angle scattering to study the effects of moisture content on a native soy protein. *Journal Applied Crystallography*, 41, 628–33.

Kealley, C.S., Rout, M.K., Dezfouli, M.R., Strounina, E., Whittaker, A.K., Appelqvist, I.A.M., Gilbert, E.P. & Gidley, M.J. (2008) Solid state structure and molecular mobility of soy glycinin as a function of moisture content. *Biomacromolecules*, 9, 2937–46.

Khurana, H.K., Cho, I.K., Shim, J.Y., Li, Q.X. & Jun, S. (2007) Application of multi bounce attenuated total reflectance Fourier transform infrared spectroscopy and chemometrics for determination of aspartame in soft drinks. *Journal of Agricultural and Food Chemistry*, 56, 778–83.

King, S.M. (1999) In *Modern Techniques for Polymer Characterisation*, (eds R A Pethrick & J V Dawkins), Chapter 7. John Wiley & Sons, Chichester.

Kinta, Y. & Hatta, T. (2005) Composition and Structure of Fat Bloom in Untempered Chocolate, *Journal of Food Science.* 70, S540–S542.

Kirby, A.R., Gunning, A.P. & Morris, V.J. (1995) Atomic force microscopy in food research: A new technique comes of age. *Trends in Food Science and Technology*, 6, 359–65.

Lalush, I., Bar, H., Zakaria, I., Eichler, S. & Shimoni, E. (2005) Utilization of amylose-lipid complexes as molecular nanocapsules for conjugated linoleic acid. *Biomacromolecules*, 6, 121–30.

Le Bail, P., Rondeau, C. & Buléon, A. (2005) Structural investigation of amylose complexes with small ligands: helical conformation, crystalline structure and thermostability. *International Journal of Biological Macromolecules*, 35, 1–7.

Le Réverend, B.J.D., Bakalis, S. & Fryer, P.J. (2008) Probing food structure. In: *Food materials science: Principles and practice* (eds J.M. Aguilera, & P.J. Lillford) pp. 203–29. Springer Science, Business Media, LLC, New York.

Liu, Y. & Guo, R. (2008) Aggregation properties of aqueous casein hydrolysate solutions at different pH. *International Dairy Journal*, 18, 1022–7.

Loisel, C., Lecq, G., Keller, G., Bourgaux, C. & Ollivon, M. (1998) Phase transitions and polymorphism of cocoa butter. *Journal of the American Oil Chemists' Society*, 75, 425–39.

Lopez, F., Samseth, J., Mortensen, K., Rosenqvist, E. & Rouch, J. (1996) Micro- and Macrostructural Studies of Sodium Deoxycholate Micellar Complexes in Aqueous Solutions. *Langmuir*, 12 (26), 6188–96.

Lopez, C., Camier, B. & Gassi, J.Y. (2007) Development of the milk fat microstructure Turing the manufacture and ripening of Emmental cheese observed by confocal laser scanning microscopy. *International Dairy Journal*, 17, 235–47.

Lopez-Rubio, A., Flanagan, B.M., Gilbert, E.P. & Gidley, M.J. (2008) A novel approach for calculating starch crystallinity and its correlation with double helix content: A combined XRD and NMR study. *Biopolymers*, 89, 761–8.

López-Rubio, A., Flanagan, B.M., Shrestha, A.K., Gidley, M.J. & Gilbert, E.P. (2008) Molecular rearrangement of starch during in vitro digestion: toward a better understanding of enzyme resistant starch formation in processed starches. *Biomacromolecules*, 9, 1951–8.

Lopez-Rubio, A. and Gilbert, E.P. (2009) Neutron Scattering: A natural Tool for Food Science and Technology Research. *Trends in Food Science and Technology*, 20, 576-58–6.

López-Rubio, A., Lagaron, J.M., Gimenez, E., Cava, D., Hernandez-Muñoz, P., Yamamoto, T. & Gavara, R. (2003) Morphological alterations induced by temperature and humidity in ethylene-vinyl alcohol copolymers. *Macromolecules*, 36, 9467–76.

Luykx, D.M.A.M., Peters, R.J.B., Van Ruth, S.M. & Bouwmeester, H. (2008) Review of analytical methods for the identification and characterization of nano delivery systems in food. *Journal of Agricultural and Food Chemistry*, 56, 8231–47.

Mannina, L., Palumi, M., Proietti, N., Bassi, D. & Segre A.L. (2001) Geographical characterisation of Italian extra virgin olive oils using high field H-1 NMR spectroscopy. *Journal of Agricultural Food Chemicals*, 49, 2687–96.

Manno, D., Filippo, E., Serra, A., Negro, C., De Bellis, L. & Miceli, A. (2009) The influence of inulin addition on the morphological and structural properties of durum wheat pasta, *International Journal of Food Science and Technology*, 44, 2218–24.

Marchin, S., Putaux, J., Pignon, F. and Léonil, J. (2007) Effects of the environmental factors on the casein micelle structure studied by cryo transmission electron microscopy and small-angle X-ray scattering/ultrasmall-angle X-ray scattering. *Journal of Chemical Physics*, 126, 1–10.

Mata, J.P., Udabage, P. & Gilbert, E.P. (2011) Structure of Casein Micelles in Milk Protein Concentrate Powders via Small Angle X-ray Scattering. *Soft Matter*, 7, 3837–43.

Mezzenga, R., Schurtenberger, P., Burbidge, A. & Michel, M. (2005) Understanding foods as soft materials. *Nature Materials*, 4, 729–40.

Michel, M. & Sagalowicz, L. (2008) Probing food structure. In: Food materials science: Principles and practice (eds J. M. Aguilera, & P. J. Lillford), pp. 203–29. Springer Science, Business Media, LLC, New York.

Monaci, L., Vatinno, R. & Benedetto, G.E. (2007) Fast detection of cyclopiazonic acid in cheese using Fourier transform mid-infrared ATR spectroscopy. *European Food Research and Technology*, 225, 585–8.

Morris, V.J., Kirby, A.J. & Gunning, A.P. (1999) *Atomic force microscopy for biologists*. Imperial College Press, London.

Morris, V.J. (2004) Probing molecular interactions in foods. *Trends in Food Science and Technology*, 15, 291–7.

Morrison, W.R., Law, R.V. & Snape, C.E.J (1993) Evidence for the inclusion complexes of lipids with V-amylose in maize, rice and oat starches. *Cereal Science*, 18, 107–9.

Noronha, N., Duggan, E., Ziegler, G.R., Stapleton, J.J., O'Riordan, E.D. & O'Sullivan, M. (2008) Comparison of microscopy techniques for the examination of the microstructure of starch-containing imitation cheeses. *Food Research International*, 41, 472–9.

Nuessli, J., Putaux, J.L., Le Bail, P. & Buléon, A. (2003) Crystal structure of amylose complexes with small ligands. *International Journal of Biological Macromolecules*, 33, 227–34.

Pawley, J.B. (2006) Fundamental limits in confocal microscopy. In: *Handbook of Biological Confocal Microscopy* (3rd ed.) (ed J.B. Pawley) pp. 19–38. Springer, Berlin.

Pawley, J.B. (2008) LVSEM for biology. In: *Biological Low Voltage Scanning Electron Microscopy* (eds H. Schatten and J.B. Pawley) pp. 27–106. Springer Science, New York.

Pedreschi, F., Aguilera, J.M. & Arbildua, J.J. (1999) CLSM study of oil location in fried potato slices. *Microscopy and Analysis*, 37, 21–2.

Perry, C.C., Weatherly, M., Beale, T. & Randriamahefa, A. (2009) Atomic force microscopy study of the antimicrobial activity of aqueous garlic versus ampicillin against *Escherichia coli* and *Staphylococcus aureus*. *Journal of the Science of Food and Agriculture*, 89, 958–64.

Pinzón-Arango, P.A., Liu, Y. & Camesano, T.A. (2009) Role of cranberry on bacterial adhesion forces and implications for *Escherichia coli*-uroepithelial cell attachment. *Journal of Medicinal Food*, 12, 259–70.

Reynolds, P.A., Gilbert, E.P. & White, J.W. (2001) High Internal Phase Water-in-Oil Emulsions studied by Small-Angle Neutron Scattering: II. The Distribution of Surfactant., *J. Phys. Chem. B*. 104, 6925–6932.

Ridout, M.J., Gunning, A.P., Wilson, R.H., Parker, M.L. & Morris, V.J. (2002) Using AFM to image the internal structure of starch granules. *Carbohydrate Polymers*, 50, 123–32.

Rieu, A., Lemaître, J.-P., Guzzo, J. & Piveteau, P. (2008) Interactions in dual species biofilms between *Listeria monocytogenes* EGD-e and several strains of *Staphylococcus aur eus*. *International Journal of Food Microbiology*, 126, 76–82.

Rogers, M.A., Tang, D., Ahmadi, L. and Marangoni, A.G. (2008) Probing food structure. In: *Food materials science: Principles and practice*. (eds J. M. Aguilera, & P. J. Lillford). Springer Science, Business Media, LLC, New York.

Rousseau, D. & Smith, P. (2008) Microstructure of fat bloom development in plain and filled chocolate confections. *Soft Matter*, 4, 1706–12.

Rossmann, A. (2001) Determination of stable isotope ratios in food analysis. Food Reviews International, 17, 347–81.

Sagalowicz, L., Leser, M.E., Watzke, H.J. & Michel, M. (2006) Monoglyceride self-assembly structures as delivery vehicles. *Trends in Food Science & Technology*, 17, 204–14.

Saguer, E., Fort, N., Alvarez, P.A., Sedman, J. & Ismail, A.A. (2008) Structure-functionality relationships of porcine plasma proteins probed by FT-IR and texture analysis. *Food Hydrocolloids*, 22, 459–67.

Sevenou, O., Hill, S.E., Farhat, I.A. & Mitchell, J.R. (2002) Organisation of the external region of the starch granule as determined by infrared spectroscopy. *International Journal of Biological Macromolecules*, 31, 79–85.

Sheppard, C.J.R. & Shotton, D.M. (1997) *Confocal laser scanning microscopy*. Taylor and Francis Group, New York.

Shim, J.Y., Cho, I.K., Khurana, H.K., Li, Q.X. & Jun, S. (2008) Attenuated total reflectance-fourier transform infrared spectroscopy coupled with multivariate analysis for measurement of acesulfame-K in diet foods. *Journal of Food Science*, 73, C426–C431.

Shukla, A., Narayanan, T. & Zanchi, D. (2009) ructure of casein micelles and their complexation with tannins. *Soft Matter*, 5, 2884–8.

Sokolova, A., Kealley, C.S., Hanley, T., Rekas, A. & Gilbert, E.P. (2010) Small angle X-ray scattering study of the effect of pH and salt on 11S soy glycinin in the powder and solution states, *Journal of Agriculture Food Chemistry*, 58, 967–74.

Staswick, P. E., Hermodson, M.A., & Nielsen, N.C.J. (1984) *Biological Chemistry*, 259, 13431–5.

Stokes, D.J. (2003) Recent advances in electron imaging, image interpretation and applications: environmental scanning electron microscopy. *Philosophical Transactions of the Royal Society A*, 361, 2771–87.

Stuart, B.H. (2005) *Infrared spectroscopy: fundamentals and applications* (ed Barbara H. Stuart). John Wiley & Sons, Chichester (West Sussex).

Svergun, D.I. & Koch, M.H.J. (2002) Advances in structure analysis using small-angle scattering in solution, *Current Opinion in Structural Biology*, 12, 654.

Svergun, D.I. & Koch, M.H.J. (2003) Small-angle scattering studies of biological macromolecules in solution. *Reports on Progress in Physics*, 66, 1735–82.

Tan, I., Flanagan, B.M., Halley, P.J., Whittaker, A.K. & Gidley, M.J. (2007) A method for estimating the nature and relative proportions of amorphous, single, and double-helical components in starch granules by 13C CP/MAS NMR. *Biomacromolecules*, 8, 885–91.

Thorvaldsson, K., Stading, M., Nilsson, K., Kidman, S. & Langton, M. (1998) Rheology and structure of heat-treated pasta dough: Influence of water content and heating rate. *Lebensmittel-Wissenschaft und Technologie*, 26, 297–311.

Topping, D. L. & Clifton, P. M. (2001) Short-chain fatty acids and human colonic function: roles of resistant starch and nonstarch polysaccharides. *Physiological Review*, 81, 1031–64.

Tromp, R.H., van de Velde, F., van Riel, J. & Paques, M. (2001) Confocal scanning light microscopy (CSLM) on mixtures of gelatine and polysaccharides. *Food Research International*, 34, 931–8.

Ubbink, J. & Krüger, J. (2006) Physical approaches for the delivery of active ingredients in foods. *Trends in Food Science & Technology*, 17, 244–54.

Utsumi, S., Matsumura, Y. & Mori, T. (1997). Structure-function relationships of soy proteins. In: *Food Proteins and Their Applications* (eds S. Damodaran and A. Paraf) pp. 257–91. Marcel Dekker, New York.

Van de Voort, F.R. (1992) Fourier transform infrared spectroscopy applied to food analysis. *Food Research International*, 25, 397–403.

Vermeylen, R., Derycke, V., Delcour, J.A., Goderis, B., Reynaers, H. & Koch, M.H.J. (2006) Gelatinization of starch in excess water: beyond the melting of lamellar crystallites. A combined wide- and small-angle X-ray scattering study. *Biomacromolecules*, 7, 2624–30.

Vincent, A. (2001) *Molecular Symmetry and Group Theory*, 2nd Ed. John Wiley & Sons, Chichester, UK.

Vodovotz, Y., Vittadini, E., Coupland, J., McClements, D.J. & Chinachoti, P. (1996) Bridging the gap: use of confocal microscopy in food research. *Food Technology*, 50, 75–82.

Westermann, S., Brüggemann, D.A., Olsen, K. & Skibsted, L.H. (2009) Spatial distribution of light-induced lipid oxidation in semi-hard yellow cheese as detected by confocal microscopy. *Food Chemistry*, 116, 756–60.

Whitney, S.E.C. Brigham, J.E., Darke, A.H., Reid, J.S.G. & Gidley, M.J. (1995) *In vitro* assembly of cellulose / xyloglucan networks: ultrastructural and molecular aspects. *The Plant Journal*, 8, 491–504.

Wignall, G.D. (1993) Small-angle neutron scattering characterization of polymers. In: *Physical properties of polymers* (eds J.E.Mark, A. Eisenberg, W.W. Graessley, L.Mandelkern, E.T. Samulski, J.L. Koenig & G.D. Wignall) pp. 424–502. ACS, Washington, DC.

Wiesendanger, R. (1998) *Scanning Probe Microscopy Analytical Methods*. Springer, Berlin.

Zemb, T. & Lindner, P. (1991) In: *Neutron, X-Ray and Light Scattering*, North Holland, Amsterdam.

Zobel, H. F. (1988) Starch crystal transformations and their industrial importance. *Starch/Staerke*, 40, 1–7.